EFFECT OF DYE-LOADING TIME ON THE PERFORMANCE OF ZnO BASED DYE SENSITIZED SOLAR CELL

by

RIDOWANUR RASHID TUSHAR

GOLAM MORTUZA MITHU

A thesis
submitted as partial fulfilment of the requirement for the degree of

BACHELOR OF SCIENCE IN ELECTRICAL AND ELECTRONIC ENGINEERING

Department of Electrical and Electronic Engineering
INTERNATIONAL ISLAMIC UNIVERSITY CHITTAGONG

JULY 2022

CERTIFICATE OF APPROVAL

The thesis entitled as **"Effect of dye-loading time on the performance of ZnO based dye sensitized solar cell"** submitted by **Ridwanur Rashid Tushar**, bearing Matric ID. **ET173081** and **Golam Mortuza**, bearing Matric ID. **ET173061** of session **Autumn 2021**, to the Department of Electrical and Electronic Engineering, International Islamic University Chittagong, has been accepted as satisfactory in partial fulfilment of the requirements for the degree of Bachelor of Science in Engineering and approved for the examination held on **JULY, 2022**.

_____

Supervisor
Dr. Md. Shamimul Haque Choudhury
Associate Professor,
Department of Electrical and Electronic Engineering
International Islamic University Chittagong.

DECLARATION

It is hereby declared that this work has been done by us and no portion of the work contained in this thesis/project has been submitted elsewhere for the award of any degree or diploma.

_____

Ridowanur Rashid Tushar

_____

Golam Mortuza Mithu

ACKNOWLEDGMENT

At the outset, we would like to express our gratitude to the Almighty, the Merciful and the Benevolent, Allah (SWT) for his benefaction and blessing on us which enabled us to complete this research.

While we were starving in doing our research and preparing this dissertation, we have got generous and spontaneous supervision, guidance and support from the following persons and hence we want to take the honor and privilege to show our gratitude to those persons. This thesis could not have been written without the great support of our supervisor, Dr. Md. Shamimul Haque Choudhury. Not only he has encouraged and motivated us throughout the whole course but also has faith in our ability to accomplish a research paper on this thesis. He has provided tremendous insights and invaluable comments on the thesis.

We would like to express our deep gratitude to him for his advice, guidance, patience and understanding throughout whole period of conducting the research. We are especially indebted to him in this regard as we got the chance to develop our skill on how to conduct research and use statistical software.

We are also thankful to the faculty members of department of EEE for their kind support in this regard. We owe to all those authors and researchers whose work we used in designing the research and in preparing this dissertation.

We want to thank all of our family members specially parents, sisters & brothers for their contributions in completing our research. We thank them all in making it possible for us to carry out this research as well as to enjoy such an enlightening experience.

Authors

ABSTRACT

Dye-sensitized solar cells (DSSCs) are one of the new photovoltaic technologies with strong commercial prospects because of their semitransparency, low production cost, simple fabrication techniques, and high performance under low-light situations. In this investigation, the effect of varying dye-loading time on photovoltaic performance for dye-sensitized solar cells has been observed using I-V Data Analysis. In the lab, the cell was fabricated using the electrophoretic deposition technique which ensures a uniform layer of metal oxide. The photoanode is immersed in the dye for 30 minutes, 1 hour, 2 hours, and 3 hours during the cell fabrication process. All the experimental procedures are done at room temperature. I-V data under dark and illumination conditions are measured with a solar simulator in the air with the area restricted by a steel mask. The values of the series resistance, shunt resistance, ideality factors, and barrier heights are calculated from the measured dark current-voltage (I-V) data using the conventional and Cheung function methods. Using the lambert W function, calculated series resistance and shunt resistance from I-V data(Illumination Condition). Under dark and illuminated conditions, 1 hr dye loading time cell has low series resistance and high shunt resistance compared to other cells. At optimum 1 hour dye-loading time cell give better performance with the conversion efficiency of 2.7%, short circuit current density of 8.9 (mA/cm^2), open circuit voltage(V_{oc}) of 0.53 (V), Fill factor(FF) of 0.56 respectively.

TABLE OF CONTENTS

LIST OF TABLES

LIST OF FIGURES

LIST OF ABBREVIATIONS

DSSC Dye Sentisized Solar Cell

FTO Flourine doped Tin Oxide

AM Air Mass

PV Photovoltaic

TCO Transparent Conductive oxide

SCR Silicon Controlled Rectifier

CHAPTER 1
INTRODUCTION

1.1 Introduction

Solar energy is unquestionably the most abundant form of energy on Earth.The development of solar cells that harness this solar energy could be sufficient to meet the rising energy demands of our society. Recent interest has increased in solar photovoltaic technology as a potential future alternative energy source. In 1991, Brian O'Regan and Michael Gratzel invented the dye-sensitized solar cell (DSSC), which consisted of a monolayer of Ruthenium dye adsorbing onto a wide band of a mesoporous semiconducting layer of Titanium dioxide (TiO_2). The ZnO-based DSSC has been extensively studied as a third-generation solar cell due to its potential for commercialization, low cost, and easy assembly. It has greater electron mobility and a lower recombination probability than TiO_2. ZnO-based solar cells can be manufactured at a cheap price using eco-friendly components such as ZnO and natural dyes extracted from locally accessible fruits and flowers. Due to the lower efficiency of ZnO-based DSSCs with natural dyes compared to silicon-based solar cells, substantial research has been conducted to reduce the cost of DSSCs while retaining their performance. Dye adsorption in ZnO nanostructures and the dye absorption spectrum [1] are among the characteristics that impact the overall performance of DSSCs. A dye-sensitized thin-film solar cell is an inexpensive member of the thin-film solar cell family. It relies on a photoelectrochemical system in which a semiconductor is formed between a photo-sensitized anode and an electrolyte. The DSSC is simple to manufacture using conventional roll printing techniques, is semiflexible and semitransparent, allowing it to be employed in a variety of applications not conceivable with glass-based systems, and the majority of its constituent ingredients are inexpensive [2]. A capacitive device is comprised of a wide band gap nanostructured semiconductor coated on a transparent conducting oxide (TCO) photoelectrode, organic dye molecules for light-harvesting, an electrolyte as a charging provider, and a catalyst (typically platinum) to activate the charges in the electrolyte deposited on the counter electrode. The interfacial properties of each component are crucial to the DSSC's performance.

Utilizing a nanostructured material is primarily intended to maximize light harvesting by

offering a high surface area for dye adsorption. Zinc Oxide (ZnO) is a promising alternative wide band gap material due to its similar band gap to TiO_2 and the ease with which it can be made in a range of nanostructures. This provides for greater flexibility in the manufacturing of DSSC solar cells, resulting in enhanced efficiency and durability [3]. Researchers have concentrated on the creation and modification of dye-sensitized solar cells (DSSCs) for converting solar energy into electricity throughout the past decade. The power conversion efficiency of ordinary silicon solar cells ranged between 10% and 34%. Even though silicon-based solar cells have excellent photovoltaic performance, their utility is constrained by the high cost of their complex manufacturing designs. Polymer-based DSSCs have been offered as a cost-effective alternative to conventional silicon solar cells on account of their better photovoltaic and optical properties and ease of production. They exhibit a high photon-to-electric conversion efficiency (11-12 percent under laboratory conditions) as well as excellent stability and long-term durability [4].

They are attractive photovoltaic devices for mass production because of their straightforward construction and potentially low production costs. In the most prevalent DSSC, a nanoparticle TiO_2 photoelectrode and a platinum counter electrode are separated by an iodide-triiodide (I-/I_3-) liquid electrolyte. Zinc oxide has lately emerged as a promising alternative to TiO2 as a semiconductor material due to tremendous performance improvements in ZnO-based DSSCs over the past several years.

In comparison to anatase TiO_2, the potential advantages of ZnO in DSSCs include rapid charge transport and orders of magnitude greater electron mobility. This property is intended to facilitate a high charge collection efficiency and facilitate the redox shuttle transition in solar cells with a greater open-circuit voltage (V_{oc}), such as [5], and to enable a high charge collection efficiency.

1.2 Objective

1. Determination of series and shunt resistance from the I-V curve of ZnO-based DSSC under illumination.
2. Determination of parameters from dark I-V curve of ZnO-based DSSC.
3. Comparison between parameters of dark I-V curve by different methods.

1.3 Outline of the Work

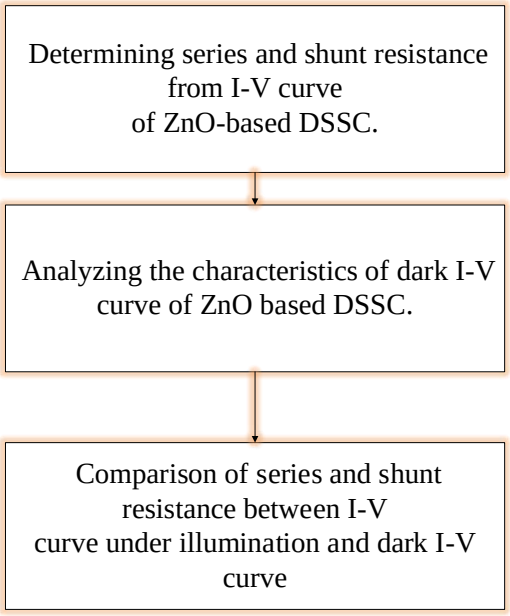

Fig. 1.1 Outline of the Work

1.4 Thesis Layout

The thesis is organized by different six chapters:

Chapter one provides a general introduction and objectives of this study.

Second Chapter this study discusses about literature review, introduction of ZnO, the underlying theories and fundamental properties of ZnO. It also explains different application of ZnO. This chapter also provides a future of ZnO.

Chapter Three gives a brief description of the parameters of dark current-voltage analysis.

Chapter Four provides the exploration of experimental work.

Chapter Five presents result and discussion regarding parameter extraction of dark current-voltage analysis of ZnO based DSSC under dark condition and series and shunt resistance determination under illumination.

Chapter Six provides conclusion of this study.

CHAPTER 2
LITERATURE REVIEW

2.1 Introduction

Dye-sensitized solar cells (DSSCs) have attracted both practical and theoretical attention since they emerged as a viable, low-cost alternative to conventional silicon-based solar cells. DSSCs, as opposed to silicon-based solar cells, employ various components for the light-harvesting and transport functions. This allows researchers to fine-tune each material and, under ideal circumstances, to optimize their combined performance in completed devices. This work poses experimental problems due to the variety of elementary components present in these cells and their numerous potential combinations. Despite the substantial experimental efforts made in their development, the photo conversion efficiencies recorded up to this moment are still poor.

2.2 Solar energy and solar cells

The need for alternative energy sources is driven by the rising global energy demand and the negative environmental effects of the past several decades' heavy use of fossil fuels. Modern society places a lot of emphasis on the creation of new technologies that enable the use of so-called renewable energy sources. Renewable energy comes from ongoing natural processes that replenish it. It is advantageous to use these energy sources from an ecological and financial standpoint. The fastest-growing source of electricity generation today is renewable energy, primarily made up of hydropower and wind power. Additionally, over the past ten years, the production of solar power has grown at an accelerated rate. According to projections, renewable energy will account for more of the world's electrical generation by 2035, up from its 2007 level of 18% [6].Therefore, it is of scientific, technological, economic, and public interest to optimize the current power generation processes and develop new technologies.

Although humanity has long used solar energy, a first attempt at photovoltaic solar energy utilization was not undertaken until the 19th century. Since then, both the scientific community and the general public have frequently discussed the idea of harnessing the free and abundant solar energy and turning it into power. Grid-connected solar systems did not, however, begin to significantly contribute to the production of electrical energy

until the early twenty-first century.

Over the past ten years, the solar industry has seen tremendous growth. Along with growing public knowledge that the world's oil sources may run out in the not too distant future, photovoltaic technology development is also aided by societal concern for the environment. Due to its comparatively low life cycle emissions of greenhouse gases, solar power generation represents a viable electric power generation technology in this regard. Governments provided incentives to encourage the use of solar energy and shift consumption away from fossil fuels to a more secure source because they were worried about climate change and energy reliance. These incentives caused the photovoltaic industry to expand at a rate of more than 30% per year during the past ten years.

Crystalline silicon modules built on bulk wafers dominate current PV module manufacture (including both large-grain polycrystalline and single-crystalline Si). These products, which made up around 85% of the market in 2009, are the primary representatives of the first generation of solar cells. The traditional representation of a traditional solar cell is the p-n junction. By doping various regions of the same semiconductor with various impurities, this junction is produced. This produces an interface between p-type and n-type materials, and as a result of the differing chemical potentials that electrons and holes have across the contact, the interface has an inherent electric field. When an electron-hole pair is formed near the interface by a photon with energy greater than the band gap, the intrinsic electric field is in favor of charge separation.

The highest power conversion possible for solar radiation using a single-junction (p-n) solar cell has been the subject of numerous theoretical computations. Under AM 1.5 illumination, the theoretical analysis of Shockley and Queisser establishes a maximum efficiency of 31% for a semiconductor with a band gap energy (E_g) of 1.3 eV [5]. There are two primary explanations for the poor maximum efficiency. First, photons of energies E are not absorbed by the solar cell. However, even electrons stimulated by photons with energy E >Eg can only supply the band gap energy (E_g) to the electric circuit, while the remainder (E-E_g) is lost due to thermal dissipation [7]. On the basis of this maximum theoretical conversion efficiency and the nature of the materials, photovoltaic cells can be categorized into three distinct generations. The first group consists of cells that utilize high-purity materials with low concentrations of structural flaws. These are the most effective cells currently available. Crystalline silicon solar cells with a proven record effi-

ciency of 25% at the time of writing [8]. belong to this category. Silicium is not a suitable semiconductor for photovoltaic conversion, despite being the most utilized and investigated material for solar conversion. It has a low optical absorption coefficient because it is an indirect semiconductor. Therefore, Si wafers with a thickness greater than one hundred microns are required to absorb the majority of incident light. This, together with the expensive purifying and crystallisation processes of silicon, makes the fabrication of silicon cells extremely costly. This category also includes binary II-IV and II-V semiconductors such as GaAs, GaAlAs, GaInAsP, InAs, InSb, and InP. They are intriguing materials for solar cells due to their near-optimal band gaps. However, these materials are quite costly. They have been utilized primarily in space solar cells, where performance trumps cost. In addition, they have a function in concentrating systems where the active surface area of the cells can be greatly reduced, allowing the use of expensive materials. Si-based photovoltaics of the first generation are a solid and proven PV technology, but their potential for cost reduction appears to be limited. In addition, although there is still opportunity for improvement, silicon solar cell efficiencies are near to the Shockley-Queisser theoretical limit for a single junction cell.

To address the issues associated with the first generation of photovoltaics, two distinct approaches have been taken: (a) to reduce costs and (b) to raise energy conversion efficiency above the Shockley Queisser limit. The primary focus of the first strategy is the development of thin-film solar cells. These devices are commonly referred to as photovoltaics of the second generation. Third-generation PV technologies, on the other hand, are predicated on strategies centered on devices that might theoretically surpass the Shockley Queisser limit.

Thin-film technology underpins the second generation of solar cells. These cells are based on a single junction and hence share the theoretical efficiency limit with the first generation of photovoltaics. Thin film devices represent a modest but constantly expanding portion of the PV industry. The development of thin film solar cells has been motivated by its potential to reduce manufacturing expenses. The most effective examples are cadmium telluride (CdTe) and copper indium gallium diselenide solar cells (CIGS). These substances are direct semiconductors; hence, just a thin coating (about 10 micrometers in thickness) is required for total light absorption. According to Shockley and Queisser, CdTe has a direct optical band gap of 1.5 eV that is close to the optimal band

gap. Additionally, thin film semiconductors may be formed on vast surfaces, which is advantageous for mass production. In contrast, PV modules based on crystalline silicon must be constructed from individual cells. However, the efficiency of second-generation devices is often lower than that of first-generation cells. In contrast to PV systems based on Si wafers, which are currently close to the theoretical efficiency limit, thin-film solar cells have yet to reach their full potential. The manufacturing phase of thin film technologies is in its infancy, and the efficiencies of small-area laboratory devices do not easily convert to the efficiencies of big modules. The greatest performance among all thin film technologies was achieved by a 1 cm^2 CIGS cell with 19.4% efficiency [8]. Use of poisonous compounds, such as cadmium, and rare elements, such as telluride and indium, are the primary difficulties associated with this technique. The introduction of a purportedly eco-friendly technology that employs toxic metals is highly controversial.

Several strategies for the third generation of solar cells have been proposed during the past few decades. The third generation encompasses numerous technologies. In general, this phrase refers to systems that do not fall into the first or second generation and/or attempt to avoid the Shockley-Queisser limit of 31%. Diverse strategies for achieving efficiency greater than 30% have been investigated. The best-known illustration of how such great efficiency could be obtained involves tandems of cells. In this instance, the conversion efficiency can be enhanced by stacking cells with varying band gaps, hence enhancing spectral sensitivity. Theoretically, by stacking a large number of suitably adapted and designed cells, efficiencies as high as 67% and 86%are theoretically achievable for unconcentrated and maximally concentrated solar irradiation, respectively.

In the 1990s, a novel method to low-cost photovoltaics based on nanostructured and organic materials was developed for solar cells. Organic heterojunctions, extremely thin absorber (ETA) cells, hybrid solar cells, and dye-sensitized solar cells are the most active research areas [9]. Since molecular and nanostructural engineering techniques can be utilized for further development, these novel solar cells offer a significant growth potential. The active layer of an organic heterojunction is composed of two materials: a donor (n-type) and an acceptor (p-type). Donors include poly-phenylenevinylene derivatives and poly-alkylthiophenes; acceptors include fullerene and its derivatives. 5.15% is the highest rate of photoconversion that has been confirmed for devices of this sort [8]. The three-phase ETA cells are composed entirely of inorganic solids. In these cells, a thin

semiconductor that absorbs light is sandwiched between two transparent, highly interconnected nanostructured semiconductors that serve as electron and hole conductors. Typically, semiconductors with a large band gap, such as TiO_2 and ZnO, are employed as electron conductors, while CuSCN is used as a hole conductor. Utilizing In_2S_3 has yielded the highest efficiencies for entirely inorganic ETA cells (3.54%) to date. In contrast to the preceding two types of solar cells, organic and inorganic components are blended in hybrid solar cells. Typically, they consist of a conjugated polymer, which absorbs light and transports holes, and an inorganic electron conductor, both of which are assembled in a heterojunction. With these sort of cells, conversion efficiencies above 5% have been attained [10]. Finally, dye-sensitized solar cells (DSCs) [11] are based on nanostructured semiconductor sheets with a large band gap that have been photosensitized with a dye. M. Gratzel & B. O'Regan reported in 1991 a device composed of sensitized nanoporous TiO_2 with a 7.1% conversion efficiency [11]. This finding opened up a new field of scientific study, and numerous research organizations have subsequently tried to enhance the efficiency and stability of these solar cells. In the recent decade, two or three research articles have been published every day in this topic [12]. At the time of writing, the record AM 1.5 efficiency for a DSC stood at 11.1% [13].

It is yet unclear which of the aforementioned technologies will influence the future of photovoltaics. Most likely, the optimal approach will rely on the specific application and other variables, such as geography. In such situation, a significant diversification of the photovoltaic market in the near future will be the most likely outcome

.

2.3 Dye Sensitized Solar Cell (DSSC)

In the future years, it is anticipated that DSSC, a potential alternative energy source, would contribute significantly more to global energy output. This is mostly owing to the low-cost fabrication and appealing characteristics, such as transparency, adaptability, etc., that may aid market penetration. DSSCS are the only devices that have demonstrated modest efficiency, making them viable competitors to conventional cells. DSSC combine optical absorption and chargeseparation processes by combining a light-absorbing sensitizer with a wide band-gap semiconductor (usually titanium dioxide). As early as the 1970s, it was found that TiO_2 from photoelectrochemical cells could split water with a small bias voltage when exposed to light [14]. As a result of TiO_2's high band gap, which

renders it transparent to visible light, the conversion efficiency was low when the sun was used as the lighting source. This innovative research includes the extending of the system's absorption range into the visible region, as well as the validation of the operating mechanism through the injection of electrons from photoexcited dye molecules into the conduction band of an n-type semiconductor. Since only a single layer of adsorbed dye molecules was photoactive, the flat surfaces of the semiconductor electrode had a low and restricted light absorption. Introducing polycrystalline TiO_2 (anatase) sheets with a surface roughness factor of several hundred resolved this issue. In 1991, cells containing mesoporous electrodes and a redox electrolyte based on an iodide/triiodide pair had conversion efficiency of 7%. The next highest energy conversion efficiency is over 11% [13], and further increase of the efficiency is possible by designing proper electrodes and sensitization dyes. Michael GrÃd'tzel l is a professor and the director of the Laboratory of Photonics and Interfaces at the Ecole Polytechnique federale de Lausanne . He pioneered research on energy and electron transfer reactions in mesoscopic-materials and their optoelectronic applications, as well as the discovery of a novel type of solar cell based on dye-sensitized mesoscopic oxide particles and the application of nanomaterials in lithium ion batteries. Today, record efficiencies in excess of 13% have been demonstrated at illumination intensities of 1000 Wm^{-2}, and the device's stability data is encouraging.

In recent years, DSSCs have been able to attain moderate conversion efficiencies of up to 14%. In this instance, mesoporous nanocrystalline TiO_2 with a large band gap was utilized as the photoanodic material, onto which dye molecules were adsorbed for photo harvesting. Recent technological advancements and optimization have largely contributed to the DSSC's major achievements. Zinc oxide (ZnO), a wurtzite-type semiconductor with an energy gap of 3.37 eV at ambient temperature, has now replaced TiO_2 as an alternate, direct large band gap metal oxide material (Table 2.1). Due to its huge bandgap, ZnO is an outstanding semiconductor material, similar to GaN and SiC, which also have broad bandgaps. **Table 2.1** Table 2.1 compares the crystal structure, energy band gap, electron mobility, and electron diffusion coefficient of nanomaterials composed of ZnO and TiO_2 . The band gap energy of ZnO nanoparticles is nearly identical to that of TiO_2 , and the electron mobility and electron diffusion coefficient of ZnO are significantly higher than those of TiO_2 , which is crucial for the application of DSSC. Extensive research

on ZnO-based DSSC technology has been conducted in order to comprehend this issue. ZnO is a wide-bandgap semiconductor with an energy-band structure and physical attributes comparable to those of TiO_2 (**Table 2.1**), but with higher electronic mobility that would be advantageous for electron transport in DSSCs, with lower recombination loss. Numerous investigations have previously been initiated and reported on the usage age of ZnO nanomaterial in DSSCs. Despite the fact that the conversion efficiencies of 0.4% to 5.8% for ZnO are significantly lower than those of 11% for TiO_2 , ZnO is still regarded as a superior alternative to TiO_2 due to its crystallization ease and anisotropic growth. Due to these qualities, ZnO may be manufactured in a vast array of nanostructures, hence presenting unique properties for electronics, optics, and photocatalysis. Simultaneously, various publications have been published that provide an in-depth examination of their shape-controllable synthesis of needles, rods, tubes, towers, hollow prisms, tetra-legs, flowers, stars, helices, belts, and springs using a straightforward technique. Due to the surface effect, quantum confinement effect, and photon localization, nanostructures with a large specific surface area are utilized for a variety of applications in electron transport and light propagation. Nanoparticles, nanorods, nanotubes, nanobelts, nanosheets, and nanotips are the predominant Nano structural forms of ZnO created during the past several decades. Sol-gel synthesis, hydrothermal/solvothermal growth, physical or chemical vapor deposition, low-temperature aqueous growth, chemical bath deposition, and electrochemical deposition are all viable methods for producing these structures.

Table 2.1 A comparison of physical properties of ZnO and TiO2

Parameter	ZnO	TiO_2
Crystal Structure	rocksalt, zinc blende, and wurtzite	rutile, anatase and brookite
Energy band gap(eV)	3.2-3.3	3.0-3.2
Electron mobility(cm$^2)Vs	205-300(bulk ZnO), 1000 (Single nanowire)	0.1-4
Refractive Index	2.0	2.5
Electron effective mass(me)	0.26	9
Relative dielectric constant	8.5	170
Electron diffusion co-efficient	5.2(bulk ZnO), 1.7 x 10^4 (nano-particulate film)	0.5 (bulk TiO_2), 10^8-10^4 (nano-particulate film)

Moreover, these ZnO nanomaterials can be synthesized via simple chemical methods

with a broad range of structural evolution; therefore, it will be prudent and reliable to fabricate DSSCs with ZnO nanostructured materials rather than TiO_2 , whose structural controllability is difficult to achieve via a conversional chemical synthetic route. Recent breakthroughs in ZnO nanostructures, notably for use in DSSCs, are detailed in this chapter. It will demonstrate that photoelectrode films containing nanostructured ZnO can significantly improve solar-cell performance by providing a large surface area for dye adsorption, direct transport pathways for photoexcited electrons, and efficient scattering-centres for improved light harvesting efficiency. In addition, the limitations of ZnO-based DSSCs are explored. In the concluding section, many attempts to extend ZnO ideas to TiO_2 are discussed in order to stimulate further improvement of DSSCs' conversion efficiency.

The abbreviations for a dye-sensitized solar cell include DSSC, DSC, and DYSC. The modern version of a dye solar cell, also known as a Gratzel cell, was co-invented in 1988 by Brian O'Regan and Gratzel cell at the University of California, Berkeley, and later promoted by the same scientists at the Ecole polytechnique federale de Lausanne (EPFL) until the publication of the first high efficiency DSSC in 1991 [11]. This invention has earned Michael GrÃd'tzel the 2010 Millennium Technology Prize.

With efficiencies of up to 13%, dye-sensitized solar cells (DSSCs) are a promising photoelectrochemical alternative to traditional Si-based solar cells. Dye sensitized solar cells (DSSCs) are regarded as promising third-generation solar cells because of their low-cost materials and technologies, environmentally friendly manufacturing process, high photon-to-electron conversion efficiency under low light intensity, and natural fabrication into flexible panels. With efficiency of up to 13%, dye-sensitized solar cells are a possible substitute for conventional silicon-based solar cells. Theoretically, the maximum conversion efficiency of DSSCs is predicted to be around 20% [15], therefore there is room for improvement in the conversion efficiency of DSSCs. Despite these benefits, DSSCs have a substantially lower maximum certified efficiency than silicon-based solar cells. TiO2, ZnO, SnO_2, Nb_2O_5, and other anode materials such as TiO_2, SnO_2, and Nb_2O_5 have been the subject of intensive research to improve the performance of DSSCs, whereas TiO_2 is the most often utilized anode material. TiO_2 nanoparticle films coated onto fluorine-doped tin oxide (FTO) layers are typically used as the photo-electrode in DSSCs due to their favorable chemical affinity and surface area for dye adsorption, as well as their fa-

vorable energy band for charge transfer between electrolytes and dye. However, the one drawback of DSSCs is that not all photo-generated electrons are able to reach the collecting electrode, as electron transport within the nanoparticle network involves a series of hops to adjacent particles and energy loss during charge transport processes reduces conversion efficiency. This trapping process causes the transport to become sluggish and scattering to increase, which dramatically increases the recombination of electrons with oxidized dye molecules, hence decreasing efficiency and oxidized redox species. In order to improve dye adsorption, it is necessary to raise the thickness of TiO_2. However, this recombination issue is exacerbated in TiO_2 nanocrystals due to a depletion layer on the surface of TiO_2 nano crystallites, and its severity increases as the photoelectrode film thickness grows. This paper suggests a ZnO-based DSSC technology as an alternative for TiO_2 in solar cells in response to this issue. Due to its strong exciton-binding energy (60 meV) and large band gap, zinc oxide has attracted considerable interest as a photo-anode in dye-sensitized solar cells (DSSCs) (3.37 eV). Resulting in an overall decrease in the dye's electron injection efficiency. There are numerous methods for increasing the efficiency of ZnO DSSCs. The introduction of a surface passivation layer to a mesoporous ZnO framework is one approach; however, this may exacerbate the dye adsorption issues. Alternately, traditional particle formations can be altered by modifying the photoanode's interior surface area and shape.The surface area and diffusion length, however, are incompatible. Increasing the photo-anode thickness enabled the fixation of a greater number of dye molecules; nevertheless, this increases the likelihood of electron recombination due to the increased distance electrons must travel to reach the transparent conductive oxide (TCO) collector. This trapping mechanism increases scattering and slows electron transit, so increasing the recombination of electrons with oxidized redox species or oxidized dye molecules, thereby decreasing efficiency. A plausible method for enhancing electron transport in DSSCs is to replace the nanoparticle photo-electrode with a single crystalline nanorod (or nanosheet, nanobelt, or nanotip) photo-electrode. Electrons can be directed along a direct electron channel within a nanorod, as opposed to being transported by multiple scattering between nanoparticles. In experiments, the electron transport in nanoparticle DSSCs is tens to hundreds of times slower than in nanorod-based DSSCs. Numerous studies have been conducted on the production of TiO and ZnO nanostructures for use in DSSCs. In addition, its electron mobility is two to

three orders of magnitude greater than that of TiO2.

Therefore, it is anticipated that ZnO will exhibit faster electron transit and less recombination damage than TiO_2. However, research indicates that the overall efficiency of TiO_2 DSSCs is greater than that of ZnO DSSCs.TiO_2 thin-passivation shell layers have a better efficiency than the best recorded efficiency of ZnO DSSCs, whose primary difficulty is the dye adsorption process. Due to the high carboxylic acid binding groups in the dyes, ZnO is dissolved and dye-Zn2+ complexes are precipitated. This effect diminishes the dye's overall electron injection efficiency. There are numerous methods for increasing the efficiency of ZnO DSSCs. The introduction of a surface passivation layer to a mesoporous ZnO framework is one approach; however, this may exacerbate the dye adsorption issues. Alternately, traditional particle formations can be altered by modifying the photoanode's interior surface area and shape.The surface area and diffusion length, however, are incompatible. Increasing the photo-anode thickness enabled the fixation of a greater number of dye molecules; nevertheless, this increases the likelihood of electron recombination due to the increased distance electrons must travel to reach the transparent conductive oxide (TCO) collector. This trapping mechanism increases scattering and slows electron transit, so increasing the recombination of electrons with oxidized redox species or oxidized dye molecules, thereby decreasing efficiency. A plausible method for enhancing electron transport in DSSCs is to replace the nanoparticle photo-electrode with a single crystalline nanorod (or nanosheet, nanobelt, or nanotip) photo-electrode. Electrons can be directed along a direct electron channel within a nanorod, as opposed to being transported by multiple scattering between nanoparticles. In experiments, the electron transport in nanoparticle DSSCs is tens to hundreds of times slower than in nanorod-based DSSCs. Numerous studies have been conducted on the production of TiO and ZnO nanostructures for use in DSSCs.

2.4 Working principle of dye-sensitized solar cells

The operation of dye-sensitized solar cells is somewhat comparable to the natural process of photosynthesis in plants. In DSSCs, a metal-containing or metal-free organic dye is absorbed into semiconductor material in place of the green, light-harvesting pigment chlorophyll. The nanostructured semiconductor with a large band gap, such as ZnO, works as the electron acceptor (similar to CO_2 in photosynthesis) by accepting electrons

in its conduction band. The I-/I3- electrolyte substitutes for water citejasim2011dye. It has been discovered that the electron injection efficiency, the degree of light absorption, and the carrier transport properties of porous nanostructured semiconductorZnO materials influence the efficiency of DSSCs.

Light absorption and excitation of the dye molecules, electron injection from the excited dye sensitizer, and conduction are the primary processes at work in DSSCs. Band of the very porous thin layer of ZnO nanoparticles with an extremely high specific surface area coated on a conducting electrode, charge collection and extraction at the conducting electrode, production of electrical energy, and regeneration of the dye molecules. When light is shone on the dye-sensitized transparent conduction ZnO layer, photoexcitation of the electrons from the highest occupied molecular orbital (HOMO) to the lowest unoccupied molecular orbital (LUMO) of the dye molecules takes place, resulting in the injection of electrons into the conduction band of the ZnO. The conduction layer (CL) is responsible for charge collection and extraction (**Fig. 2.1**). This removed charge generates electrical work in the external circuit (Equations 1-3).

$$Dye + h\nu \rightarrow Dye^{*} \tag{2.1}$$

$$Dye^{*} + ZnO \rightarrow ZnO(e^{-}) + Dye^{+} \tag{2.2}$$

$$ZnO(e^{-}) + Cl \rightarrow ZnO + Cl^{-} + ElectricalEnergy \tag{2.3}$$

$$Dye^{*} + \frac{3}{2}I^{-} \rightarrow Dye + \frac{1}{2}I_{3}^{-} \tag{2.4}$$

$$\frac{1}{2}I_{3}^{-} + Cl^{-} \rightarrow \frac{3}{2}I^{-} + Cl \tag{2.5}$$

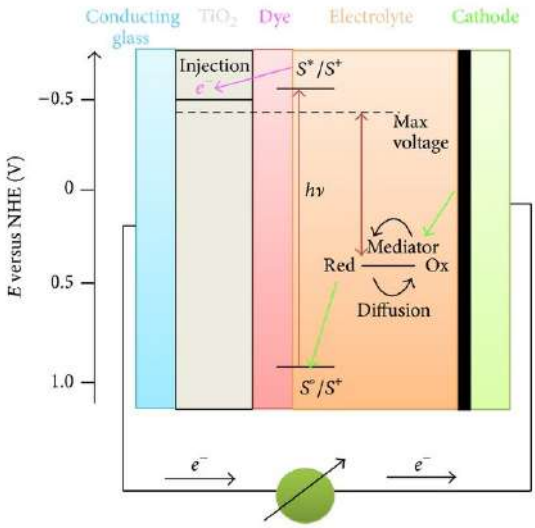

Fig. 2.1 Schematic representation of the working principle of ZnO-based DSSC

2.5 Basic structure of dye-sensitized solar cells

2.5.1 Components of DSSCs

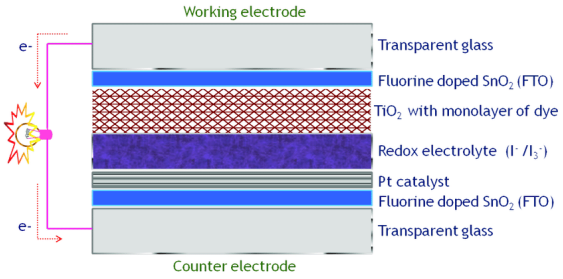

Fig. 2.2 Structure of DSSC

The conversion of light energy into electricity by DSSC is based on the sensitization of wide band gap semiconductors and comprises primarily of dye, photo electrodes, electrolyte, counter electrodes, and glass substrates with a layer of transparent conductive oxide (TCO). Each of them must be optimized in order to increase overall efficiency.

2.5.2 Photosensitizer

An efficient photosensitizer has several basic fabrication requirements including:

1. Strong dye adsorption particles onto the semiconductor surface.
2. Large visible light harvesting capacity.
3. Injection of electron efficiently into the semiconductors conduction band.
4. Lastly, – O or – OH groups with anchoring capability on TiO_2 surface, ensuring high rates in transfer of electron.

Dye plays an essential role in solar energy absorption and conversion. Numerous studies have concentrated on the molecular engineering of various inorganic metal complexes and organic colors. Transition coordination complexes are utilized as charge transfer sensitizers, converting around 11% of the solar energy in a standard global air mass AM 1.5 to electric energy. These complexes are also among the most effective sensitizers due to their higher efficiency, chemical stability, and favorable photo-electrochemical characteristics, among other attributes. However, Ru complexes contained heavy metals that are environmentally toxic, in addition to their complex and costly synthesis. In addition, Ru complexes tend to breakdown in the presence of water. Gratzeland and his team created a large number of Ru Complex Photosensitizers, which are the most effective sensitizers ($\approx 11\%$) due to their broad range of absorption from the visible to the near-infrared spectrum. Ru complexes, despite their chemical stability and the possibility of charge exchange with semiconducting substances, have a high visible light harvesting capacity, making them an excellent candidate for the production of solar energy conversion devices.

2.5.3 Electrolytes

The electrolyte plays a crucial function in the DSSC by facilitating charge transport between the photoelectrode and counter electrode. Ideal electrolyte solvents have low vapor pressure, extremely low viscosity, high dielectric characteristics, and a high boiling point. From an industrial standpoint, factors such as ease of processing, durability (chemical inertness), and environmental sustainability are also essential. Currently, the most effective redox mediator in DSSC consists of a liquid electrolyte comprising the redox couple iodide/triiodide. The redox electrolyte contains iodine, iodides, and frequently other additions. Ionic liquids are intriguing alternatives to conventional electrolytes due to their great thermal and chemical stability, non-volatility, and excellent ionic conductivity. Finding a superior redox pair is one of the primary difficulties facing future research on DSSCs.

2.5.4 Conductive Glass or Substrates

Clear conductive glasses are typically used as substrates due to their comparatively low cost, plentiful availability, and great optical quality. Thin transparent conductive oxide is deposited on one side of the substrate to provide a conductive coating (TCO). This layer is essential because it allows sunlight to enter the cell and conducts electron carriers to the

outside circuit. At normal temperature, the electrical resistance of the conductive material is between 10 and 20 Omega per square. On the conducting side, the nanostructured wide band gap oxide semiconductor (electron acceptor) is applied

2.5.5 Photo-Electrode

A DSSC's photo-electrode consists of a nanostructured semiconductor material adhered to a transparent conducting substrate. TiO_2 is the most popular semiconductor material because it is affordable, non-toxic, and abundant. The electrode is composed of linked nanoparticles ranging in size from 15 to 30 nm. They resemble a translucent porous electrode with a thickness of 10 to 15 μm. Screen printing and doctor blading are the most often used deposition processes for film preparation. Before the sintering process, both approaches include the deposition of viscous colloidal TiO_2 onto a substrate. Typically, sintering is performed at temperatures between 450 and 500 degrees Celsius. The nanoparticles become electrically interconnected as a result of the high temperature, finally forming the nanostructure porous electrode. The dye is sensitized by dipping the electrode in a dye solution for a period of time.

2.5.6 Counter Electrode

The counter electrode is a crucial component of DSSC, where mediator reduction occurs. It consists of fluorine-doped tin oxide (FTO) and platinum-coated glass to enable more reversible electron transport. The counter electrode facilitates the flow of electrons from the external circuit to the redox electrolyte. In addition, it assists to transport photocurrent over the breadth of each solar cell. For redox pair reduction, the counter electrode must conduct effectively and have a low overvoltage. Until recently, platinum (Pt) was the material of choice for the counter electrode due to its superior performance in I_3^- reduction. Until recently, platinum (Pt) was the material of choice for the counter electrode due to its superior performance in I_3^-. reduction.

2.6 ZnO

The formula for the inorganic compound zinc oxide is ZnO. ZnO exists as a white powder that is insoluble in water. As an additive, it is utilized in several materials and goods, including rubbers, plastics, ceramics, glass, cement, lubricants, paints, ointments, adhesives, sealants, pigments, meals, batteries, ferrites, fire retardants, and first-aid tapes. As the mineral zincite, zinc oxide exists naturally, although most of it is manufactured in a

laboratory. ZnO is an II-VI group semiconductor with a broad bandgap. n-type doping is the doping that occurs naturally in a semiconductor due to oxygen vacancies or zinc gaps. This semiconducting material possesses numerous advantageous characteristics, including high electron mobility, a wide bandgap, and intense luminescence at ambient temperature. These qualities are useful for new applications such as transparent electrodes in liquid crystal displays, energy-saving or heat-blocking windows, and thin-film transistors and light-emitting diodes in electronics [16].

2.6.1 Basic physical parameters for ZnO

The basic physical parameters of ZnO were compiled and placed as in Table 2.2 [17], [18].

Table 2.2 Physical Parameter of ZnO

Physical Parameter	**Values**
Stable phase at 300k	Wurtzite
Energy band gap	3.37 eV, Direct
Density	5.606 g/cm^3
Refractive index	2.008, 2.029
Melting point	1975^{o}
Thermal Conductivity	0.6, 1-1.2
Excitation binding energy	60meV
Electron effective mass	0.24
Electron Hall mobility at 300k for low n-type conductivity	200 cm^2 / V s
Linear expansion coefficient	a_o: 6.5 x $10^{-}6$ and c_o:3.0 x $10^{-}6$
Static dielectric constant	8.656
Hole effective mass	0.59
Hole Hall mobility at 300K for low p-type conductivity	5-50 cm^2/V s
Intrinsic barrier concentration	<106c^2(max n-type doping >1020$cm^{-}3$ electron, max p-type doping <1017 $cm^{-}3$ holes)
Lattice parameters at 300k	0.541nm
a0	0.32465nm
c0	0.52069nm
a0/c0	1.602
U	0.345

The physical parameters include energy band gap, excitons binding energy, electron effective mass, hole effective mass, hole hall mobility and lattice parameter for easy un-

derstanding. It should also be noted that there still exists uncertainty in some of these values. For example, there have few reports of p-type ZnO and therefore the hole mobility and effective mass are still in debate. Similarly, the values for thermal conductivity show some spread in values and this may be a result of the influence of defects such as dislocations, as was the case for GaN. The values for carrier mobility will undoubtedly increase as more control is gained over compensation and defects in the material.

2.6.2 Mechanical properties

ZnO is a relatively soft material with approximate hardness of 4.5 on the Mohs scale. Its elastic constants are smaller than those of relevant III-V semiconductors, such as GaN. The high heat capacity and heat conductivity, low thermal expansion and high melting temperature of ZnO are beneficial for ceramics.The E2 optical phonon in ZnO exhibits an unusually long lifetime of 133 ps at 10 K . Among the tetrahedrally bonded semiconductors, it has been stated that ZnO has the highest piezoelectric tensor, or at least one comparable to that of GaN and AlN. This property makes it a technologically important material for many piezoelectrical applications, which require a large electromechanical coupling [19].

2.6.3 Electrical properties

ZnO has a straight band gap of 3.3 eV at ambient temperature, which is quite large compared to other materials. The benefits of a big band gap consist of greater breakdown voltages, the capacity to withstand huge electric fields, reduced electronic noise, and high-temperature and high-power functioning. By alloying ZnO with magnesium oxide or cadmium oxide, the bandgap can be adjusted to between 3-4 eV. Even in the absence of purposeful doping, most ZnO has n-type character. The origin of n-type characteristics is often nonstoichiometric, but the question remains contentious. On the basis of theoretical calculations, it has been claimed that inadvertent substitutional hydrogen impurities are to blame. By substituting Zn with groupIII elements such as Al, Ga, or In, or by exchanging oxygen with chlorine or iodine, it is simple to accomplish n-type doping with precise control. Doping ZnO to the p-type remains tough. This issue stems from the limited solubility of p-type dopants, which is compensated for by an abundance of n-type impurities. This issue is seen with GaN and ZnSe. Sample heterogeneity complicates the measurement of p-type in "intrinsically" n-type material.

Group I elements Li, Na, and K; group V elements N, P, and As; and copper and silver are

known p-type dopants. Many of them, however, form deep acceptors and do not exhibit appreciable p-type conduction at ambient temperature. The highest electron mobility of ZnO is 2000 cm2/(V.s) at a temperature of 80 K. The electron mobility of ZnO varies significantly with temperature and reaches its maximum at 80 K. There are few data on hole mobility, with values ranging from 5 to 30 cm2/(V.s). As a varistor, ZnO discs are the active material in the majority of surge arresters. [20].

2.6.4 Limitation on ZnO-based DSSCs

Even though ZnO has strong electron mobility, a low combination rate, abundant nanostructures, and nearly the same band gap and band position as TiO_2 , the light conversion efficiency of ZnO-based DSSC is still limited. a) the creation of Zn^{2+}/dye complex in acidic dye and b) the delayed electron-injection flow from dye to ZnO are primarily responsible for the inferior performance of ZnO-based DSSCs. Zn^{2+}/dye complex production happens predominantly when ZnO is immersed in an acidic dye solution for an extended period of time. Ru-based dye molecules have a carboxylic functional group for coordination, with acidic medium constituting the majority of the dye solution. The Zn^{2+}/dye complex is hence inevitable. The production of Zn^{2+}/dye complex has been attributed to the dissolution of surface Zn atoms in an ethanolic solution by protons released from the dye molecules. ZnO material using Ru-based dyes is reported to have a poorer electron-injection efficiency compared to TiO_2 . In ZnO, the electron injection is dominated by slow components, whereas in TiO_2 it is dominated by fast components, resulting in an injection rate constant that differs by more than 100 times. In either ZnO or TiO_2 , for instance, the injection of electrons from Ru-based dyes into a semiconductor exhibits similar kinetics, with a quick component of less than 100 fs and a longer component on a picosecond time scale. In other words, the ZnO conduction bands are produced predominantly from the empty s and p orbitals of Zn^{2+}, whereas the TiO_2 conduction bands are derived mostly from the empty 3d orbitals of Ti^{4+}. The change in band structure results in a different density of states and, presumably, different electronic coupling strengths between the adsorbate and the semiconductor.

2.6.5 Application of ZnO

Each property of ZnO has a unique set of applications. ZnO's large band gap enables the formation of nanocrystal clusters and nanowires. Due to the huge band gap, the synthesis of p-n homojunctions has also been reported in numerous publications. Numerous

accurate optical devices can be constructed utilizing ZnO's 60 meV free-exciton binding energy, as ZnO's huge exciton binding energy permits it to remain stable at normal temperature and higher temperatures. ZnO crystals and thin films can be used to create nonlinear optical devices due to their second- and third-order nonlinear optical properties. In general, the advantage of fine-tuning the physical properties of various oxides, such as zinc oxide, propels the development of smart application devices [21]. By permuting and combining their two primary structural features, the electrical, optical, magnetic, and chemical properties of cations with mixed valence states and anions with deficiencies can be fine-tuned (vacancies). Figure 2.16 is a summary of the various applications of ZnO [22].

2.7 Scale-up and commercialization of dye-sensitized solar cells

DSSCs are not just the subject of scientific study. More than one hundred industrial laboratories throughout the world are working on the development of solar devices based on DSC technology. DSC technique has several distinct benefits over other photovoltaic devices. The pricing is the first and likely most alluring factor for practical applications. In comparison to conventional photovoltaic technology, DSC technology shares the cost advantage of all thin-film devices. It uses non-toxic ingredients and avoids expensive production processes (such as high vacuum, high temperature, and clean-room requirements). However, as will be explored in greater detail below, there are still some potential fabrication cost barriers, such as the price of the transparent conducting oxides used as substrate and of the precious metal-based dyes. To successfully compete with existing technologies, the new DSC technology must meet or exceed a particular efficiency thre-
Although record efficiencies exceeding 11% have been achieved in the lab for small cell areas (usually sub-centimeter range), these values drop to roughly 8% as a result of scaling up the area within a working module (25-100 cm^2). In addition, the fact that after more than 20 years of research, the record efficiency is not much higher (11% [13]) than the one reported by Gratzel and O'Regan (7%) [11]) in the Nature article that opened the dye-sensitized solar cell research field is a highly controversial topic.

Long-term stability is another important factor for industrial success. DSC stability is a very contentious topic and one of the technology's weaknesses. For a device to last 20 years, its components must resist millions of rotations. In addition, like with any photovoltaic device, they must withstand extremely high temperatures, which might cause the

dye-TiO_2 system to undergo structural alteration. Sealing is another key aspect in stability. Even in their typical forms, DSSCs are liquid-based devices. The sealing materials must prevent the electrolyte from evaporating and the accumulation of H_2O within the cell. Likewise, the sealing material must be chemically compatible with the solvent and electrolyte components. Several successful testing of solar cells under outdoor settings have been conducted, and the industrialization of DSSCs is in progress to address these challenges. Over 20,000 hours of simulated sunshine at an average light level comparable to 0.8 sun, the stability of DSCs was evaluated. Dyesol, an industrial DSC business, published accelerated aging experiments that suggested a minimum service life of 25 years in the climatic circumstances of southern Europe. The substitution of organic solvents with nonvolatile solvents is an extremely promising strategy for meeting such stringent stability requirements. In this thesis, the stability of DSSCs and the usage of non-volatile electrolytes, such as those based on ionic liquids, have received specific consideration.
The use of a dye derived from a valuable metal is a further contentious topic regarding the industrialisation of DSC technology. Ruthenium is relatively uncommon, and the market's tiny scale contributes to its price volatility. However, the hunt for alternative dyes is a highly active topic, and pure organic sensitizers have achieved yields comparable to that of ruthenium complexes. Given the modest amount used, however, the contribution of ruthenium to the total cost of the device is less than 0.01 ϵ/pWatt [23]. Currently, the clear conducting oxide substrate is the DSC component that has the greatest impact on the final pricing of this technology (TCO). Fluorine- and indium-doped tin oxides are the most widely used TCOs. The pricing and availability of these TCOs depend substantially on the demand and supply of Sn. Consequently, alternatives to Sn-based TCOs must be investigated. DSSCs are compatible with a variety of backing materials, such as flexible ones. In addition to the obvious adaptability advantages of flexible substrates, they also give a major benefit to mass production: unlike glass, flexible substrates may be utilized in continuous roll-to-roll operations, enabling a large and cost-effective production. Currently, DSCs cannot compete with other photovoltaic technologies for usage in grid-connected solar farms. In solar farms, photovoltaic devices are intended to operate under optimal orientation and relatively high light intensities. These conditions are more conducive to conventional PV. However, while operating at low intensities or high temperatures, silicon panels experience a significant loss of efficiency in contrast, DSCs

function exceptionally well under conditions equal to 0.2 to 0.5 sun, and their efficiencies are almost independent of temperature between 25 to 65 degrees Celsius [16]. Across the same temperature range, the efficiency of Si solar cells decreases by roughly 20% [16]. In addition, typical silicon technologies are far more sensitive to incidence angle than DSCs. DSCs have a high tolerance for partial shading and operate well in diffuse light illumination or hazy environments. The integration of DSCs into building architecture (a sector known as Building Integrated Photovoltaic Applications, or BIPV) is one of the most intriguing applications for this new technology due to the combination of the aforementioned qualities. Due to their heavy reliance on angle of incidence and direct light illumination, first- and second-generation solar cells are only effective for roofs. However, DSCs are also acceptable for some applications where the incidence angle is not optimal, such as on facades. DSCs also offer aesthetic benefits, such as a large variety of possible colors, nonreflectivity, and partial optical transparency. The second principal application for dye-sensitized solar cells is as an alternative to batteries for stand-alone electrical devices, such as mobile phone chargers and decorative items. Significant characteristic of these items is their short product life (up to five years, approximately). Due to the less stringent stability criteria, this allows for a greater variety of material options. Competing with flexible amorphous silicon, flexible DSCs are ideally suited for this type of application. DSCs are distinguished by their customizable color options, large variety of forms, low-light performance, good performance in diffuse light, and higher average performance over the light spectrum. Table 2.3 provides a summary of some of the developing application areas for DSCs and the primary firms working on this technology.

Table 2.3 Some application areas of DSCs under development in Various Countries

Companies	Type of application
Sharp,Sony,Nanomax,IPP,FIS	Large area solar panels for terrestrial power generation
Dyesol Italian BOPV Company , Color-sol project of Germany	BIPV
Dyesol	Flexible Power Plastics
3G Solar of Israel	power generation for remote area needs
SJC-Shimane Inst. of Industrial Tech	Street Lights and road signs
Sony's self power lamp shades	Consumer Household electronics

DSC technology is advancing rapidly toward commercial practicality. However, a number of obstacles must be addressed before it can compete with other photovoltaic technologies.

CHAPTER 3

METHOD DESCRIPTION

3.1 Introduction

In this chapter, we described the followed method for analyzing the I-V data under dark and illumination conditions. to analyze dark condition I-v data we follow the conventional method, Cheung function method, norde plot function method, and generalized norde plot function method. To analyze I-V data illumination data we followed the lambert solar cell law function.

3.2 Conventional method

If thermionic emission is the dominating process, the relationship between current and voltage for Schottky diodes is as follows:

$$I = AA^{*}T^{2}\exp(-\frac{q\varphi_b}{K_BT})[\exp(\frac{(q(V-IR_s))}{K_BT})-1] \tag{3.1}$$

Here,

A=Constant Area

φ_b= Schotty barrier height

K_b=Boltzmann's Constant

Q=Elementary charge

T=Absolute temperature in kelvin

Rs = series resistance

A^* = Richard constant

$$A^{*} = \frac{4\pi q m^{*} K^{2}}{h^{3}} \tag{3.2}$$

In equation 3.2 is Richard constant where,

m^*=effective mass carrier

h= planck constant=$6.634*10^{-34}$ j/s

A bias dependent Schottky Barrier Height and other effects which cause the deviation

from thermionic emission are included by addition of an ideality factor (n) to Equation one. The relationship between n and φ_b is given by the following expression [24]:

$$\varphi_0 = \varphi_{b0} + (1 - \frac{1}{n})V \tag{3.3}$$

Here,

φ_{b0}=Barrier Height under zero Bias.

For V-IRs>3kT/q, we can write from eq-3.1 and eq 3.3 is:

$$I = I_s \exp[\frac{qV}{nK_BT}] \tag{3.4}$$

Here,

N=Ideality factor

I_s=Saturation Current

K_B=Boltsman's constant

T=absolute temperature

V= applied voltage

In equation four was fitted at the lower part of the dark forward I-v curve in the region (V<0.4V). the saturation current was obtained by extrapolating the linear region of the curve to zero applied voltage. The saturation current Is is given by [25]:

$$I_s = AA^*T^2 \exp(-\frac{q\varphi_b}{K_BT}) \tag{3.5}$$

From equation 3.4, we can write,

$$\ln(I) = \ln(I_s) + (\frac{qV}{nKT}) \tag{3.6}$$

At low and intermediate voltage regions, by using equation (06) the plot of the (lnI-V) plot is linear and the extrapolating of this plot to the lnI axis gives the reverse saturation current Is.

The ideality factor can be determined from the slope of the plot according to the following equation:

$$n = \frac{q}{KT}(\frac{dV}{d\ln(I)}) \tag{3.7}$$

Also, zero bias barrier height which is expressed by [24]:

$$\varphi_{b0} = \frac{K_B T}{q} \ln(\frac{AA^* T^2}{I_s}) \tag{3.8}$$

Dark (I-V) parameter under forward and reverse bias at room temperatures for the diode can be obtained by semilogarithmic plot. Semilogarithmic plot is obtained by converting current (I) in to log10(I).

3.2.1 Methods of finding series and shunt resistances

To determine the series resistance and shunt resistance of a solar cell from its I-V data under dark conditions, we must first calculate Rj=dv/di and then plot Rj vs voltage. Both series and shunt resistance are denoted by Rj. The high value of this graph indicates series resistance, while the low value indicates shunt resistance.

In the case of reverse bias potential, the Rj versus Voltage plot can be used to determine the shunt resistance. In addition to forward bias potential, the same plot can be used to determine series resistance.

3.3 Cheung Function Method

It is a different kind of method to determine the ideality factor, barrier height, and Schottky diode series resistance from an I-V curve under bias conditions. . it is based on modified TE model [26].

Following the equation known as cheung function:

$$\frac{dV}{dlnI} = IRs + \frac{nKT}{q} \tag{3.9}$$

$$H(I) = V - \frac{nKT}{q} \ln \frac{1}{AA^* T^2} \tag{3.10}$$

$$H(I) = IRs + n\varphi_b \tag{3.11}$$

dV/dlnI and H(I) versus I plots are drawn using data determined from the downward curvature region of the lnI-V plot, which should be linear, when the above equations are considered. Rs is calculated using the slope of these plots. The values of n and b are derived from the y-intercept of the dV/dlnI and H(I) versus I plots, respectively.

3.4 Norde plot

H. Norde proposed this method to determine barrier height and series resistance of schotty diodes.F(v)- Voltage plot from I-V data using following equation [27]:

$$F(V) = \frac{V}{2} - (\frac{KT}{q}) \ln(\frac{I}{AA^* t^2}) \tag{3.12}$$

$$\varphi_B = F(V_o) + \frac{V_o}{2} - \frac{KT}{q} \tag{3.13}$$

Here,

$F(V_o)$= minimum value of F(V)

V_o, I_o= correspong Voltage and current of $F(V_O)$

$$F(V_o) = \frac{V_o}{2} - \frac{1}{\beta}(\frac{I_o}{AA^* T^2}) \tag{3.14}$$

To calculate the series resistance, use the equation below:

$$R_s = \frac{KT}{qI_o} \tag{3.15}$$

3.5 Generalized Norde Plot

Bohlin proposed the generalized norde function to calculate Rs and shi-b values from a single I-V measurement at a fixed temperature. The generalized Norde function is described as [28]

$$F(V, \alpha) = \frac{V}{\alpha} - \frac{1}{\beta} \ln(\frac{I(V)}{AA^* T^2}) \tag{3.16}$$

I(V) is taken from the observed I-V curve, and alpha is defined as a random constant bigger than n. Beta is equal to q/kT. By calculating F(V,alpha) against the minimum of the V plot using the following equations, Shi-b and Rs values can be found:

$$\varphi_b = F_{min}(V, \alpha) + \frac{\alpha - n}{n}(\frac{V_{min}}{\alpha} - \frac{1}{\beta}) \tag{3.17}$$

$$R_s = \frac{\alpha - n}{\beta I_{min}} \tag{3.18}$$

Where n is determined by the lnI-V plot. Fmin(v,alpha) is the minimum point on the F(V, alpha)-V graph, whereas Vmin and Imin are the minimum voltage and current, respectively.

3.6 Lambert W Function

It is a build fuction of origin pro Software used to determine series and shunt resistance from I-V data under illumination condition.this function only apply when I-V data collect in room temperature.

$$I = I_{ph} - \frac{V + IR_s}{R_{sh}} - I_s(e^{\frac{V+IR_S}{nV_{th}}} - 1) \tag{3.19}$$

Where,

$$V_{th} = \frac{kT}{q} \tag{3.20}$$

k=Boltzmann Constant

q=Electron Charge

It can be expressed using Lambert W function.

$$y = \frac{R_{sh}(I_s + I_{ph}) - x}{R_s + R_{sh}} - \frac{nV_{th}}{R_s} LambertW(\frac{R_s R_{sh} I_s}{nV_{th}(R_s + R_{sh})} e^{\frac{R_{sh}(R_s(I_s+Iph)+x)}{nV_{th}(R_s+R_{sh})}}) \tag{3.21}$$

CHAPTER 4

PARAMETER DESCRIPTION

4.1 Introduction

In this chapter, we describe the Dye sensitized solar cell performance-measuring parameters. The series resistance is the most important performance metric of a solar cell. The efficiency of power conversion also depends on series and shunt resistance. Due to the solar cell's high series resistance, its ideality factor is also high.

4.2 Saturation current

The saturation current (or scale current), more accurately, the reverse saturation current, is that part of the reverse current in a semiconductor diode caused by diffusion of minority carriers from the neutral regions to the depletion region. This current is almost independent of the reverse voltage.

I_S, the reverse bias saturation current for an ideal p-n diode, is given by:

$$I_s = eAn_i^2\left(\frac{1}{N_D}\sqrt{\frac{D_p}{\tau_p}} + \frac{1}{N_A}\sqrt{\frac{D_n}{\tau_n}}\right) \tag{4.1}$$

where,

e=is elementary charge

A= the cross-sectional area

D_p, D_n = diffusion coefficients of holes and electrons, respectively.

N_D, N_A = donor and acceptor concentrations at the n side and p side respectively.

n_i =the intrinsic carrier concentration in the semiconductor material.

τ_p , τ_n are the carrier lifetimes of holes and electrons, respectively.

Increase in reverse bias does not allow the majority charge carriers to diffuse across the junction. However, this potential helps some minority charge carriers in crossing the junction. Since the minority charge carriers in the n-region and p-region are produced by thermally generated electron-hole pairs, these minority charge carriers are extremely temperature dependent and independent of the applied bias voltage. The applied bias voltage acts as a forward bias voltage for these minority charge carriers and a current of

small magnitude flows in the external circuit in the direction opposite to that of the conventional current due to the moment of majority charge carriers. Note that the saturation current is not a constant for a given device; it varies with temperature; this variance is the dominant term in the temperature coefficient for a diode. A common rule of thumb is that it doubles for every 10 degree celsius rise in temperature [29]. Saturation current (I0) of a p-n junction solar cell are an indication of the quality of the cell. This parameter are usually estimated from dark current-voltage measurements [30].

4.3 Darkcurrent

In electronic engineering, dark current is the relatively small electric current that flows through photosensitive devices such as a photomultiplier tube, photodiode, or charge-coupled device even when no photons are entering the device; it consists of the charges generated in the detector when no outside radiation is entering the detector. It is referred to as reverse bias leakage current in non-optical devices and is present in all diodes. Physically, dark current is due to the random generation of electrons and holes within the depletion region of the device. The charge generation rate is related to specific crystallographic defects within the depletion region. Dark-current spectroscopy can be used to determine the defects present by monitoring the peaks in the dark current histogram's evolution with temperature. Dark current is one of the main sources for noise in image sensors such as charge-coupled devices. The pattern of different dark currents can result in a fixed-pattern noise; dark frame subtraction can remove an estimate of the mean fixed pattern, but there still remains a temporal noise, because the dark current itself has a shot noise [25]. When one applies a bias to a diode in the dark, a current flow through it. By applying the bias, electrons are injected at the n-type contact into silicon. This implies

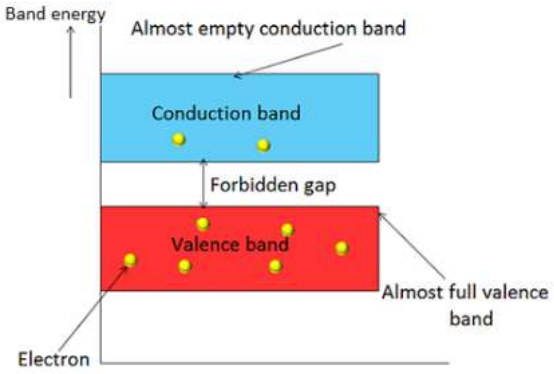

Fig. 4.1 Jumping of electron from conduction band to valance band

that the electrons, injected at the n-type contact, are able to exit through the p-type contact only if they jump down from the conduction to the valence band somewhere in the cell. In other words, only those electrons can pass through the cell that recombine somewhere in the cell. This behavior is shown in the **Fig. 4.1**. The minority carrier density increases exponentially with applied bias, and because the recombination rate is proportional to p-n, the recombination rate increases exponentially with applied bias. Since all the current that passes through the cell is recombination, the current through the cell increases exponentially with applied bias in the dark. See the **Fig. 3.2** [31] We can calculate the

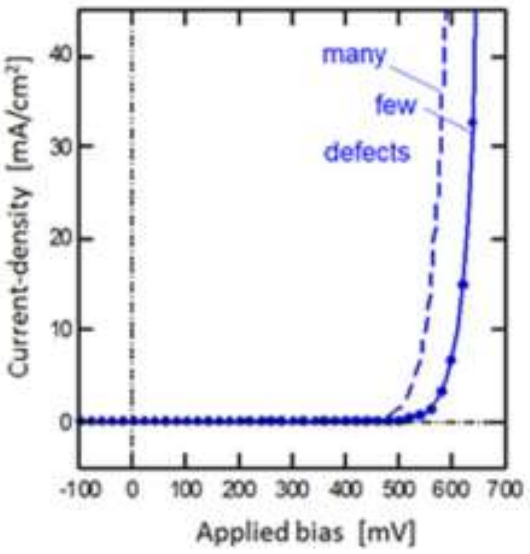

Fig. 4.2 Dark Current Voltage Curve

dark current of SCR by using the following process and equation. When the p-n junction diode in **Fig. 4.3** is forward biased, the built-in potential barrier is lowered. **Fig. 4.3** shows the components of the recombination current when the junction is forward biased and **Fig. 4.4**, the corresponding energy band diagram. The forward bias voltage, V, produces an injection of minority carriers into both sides, that is, electrons (filled circles) from the n-side into the p-side. The electrons in the p-side of the junction move by diffusion until they recombine with holes (empty circles). This recombination may take place either at the surface or in the bulk of the p-type material. This movement by diffusion of electrons in the p-side forms one component of the dark diode current (I_{D1}) in the solar cell. Similarly, the current resulting from diffusion of holes in the n-side is denoted by I_{D2}. The total diffusion current in the n- and p-regions ($I_{D1} + I_{D2}$), which also constitutes ideal recombination, is given by the Shockley equation [4.2,4.3]:

$$I_D1 + I_D2 = I_01[e^{\frac{qv}{nKT}} - 1] \tag{4.2}$$

Where, I_01 = reverse saturation current corresponding to the diffusion and recombination of electron and holes in the pond n-regions, respectively; n = ideality factor = 1; k = BoltzmannâĂŹs constant; T = absolute temperature. The last component of the dark current is a result of recombination of electrons and holes in the SCR, I_{D3}. This current constitutes non-ideal recombination and is given by

$$I_D3 = I_01[e^{\frac{qv}{nKT}} - 1] \tag{4.3}$$

Where, I_02 = reverse saturation current corresponding to the generation and recombination of electron and holes in the SCR region; n = ideality factor > 1; The total dark current comprises the components given in (3.2) and (3.3):

$$I_D = I_01[e^{\frac{qv}{nKT}} - 1] + I_02[e^{\frac{qv}{nKT}} - 1] \tag{4.4}$$

Equation (3.4) can be written as a single exponential formula:

$$I_D = I_0[e^{\frac{qv}{nKT}} - 1] \tag{4.5}$$

Where, I_0 = reverse saturation current governed by diffusion and recombination of electron and holes; n=1 if the dark current, I_D, is solely determined by diffusion; and n > 1 if recombination in the SCR also contributes to I_D .

4.4 Series resistance

Series resistance in a solar cell has three causes: firstly, the movement of current through the emitter and base of the solar cell; secondly, the contact resistance between the metal contact and the silicon; and finally, the resistance of the top and rear metal contacts. The main impact of series resistance is to reduce the fill factor, although excessively high values may also reduce the short-circuit current.

$$I = I_L - I_0 \exp[\frac{q(V + IR_s)}{nKT}] \tag{4.6}$$

Where, I is the cell output current, I_L is the light generated current, V is the voltage across the cell terminals, T is the temperature, q and k are constants, n is the ideality factor, and R_S is the cell series resistance. The formula is an example of an implicit function due to the appearance of the current, I, on both sides of the equation and requires numerical methods to solve. A schematic of series resistance is shown in **Fig. 4.3**.The effect of the series resistance on the IV curve is shown in **Fig. 3.4**

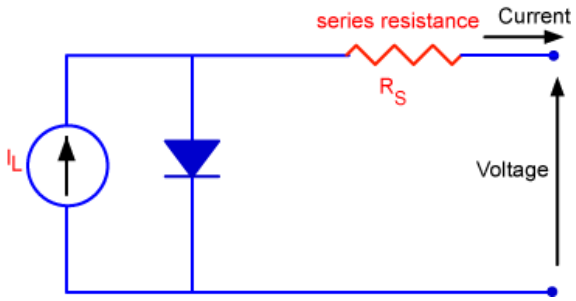

Fig. 4.3 Schematic of a solar cell with series resistance

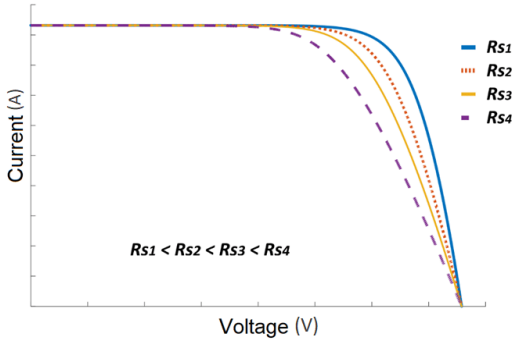

Fig. 4.4 Effect of series resistance on I-V curve

The area of the solar cell is 1 cm^2 so that the units of resistance can be either ohm or $ohmcm^2$. The short circuit current (I_{SC}) is unaffected b the series resistance until it is very large. Series resistance does not affect the solar cell at open-circuit voltage since the overall current flow through the solar cell, and therefore through the series resistance is zero. However, near the open-circuit voltage, the IV curve is strongly affected by the series resistance. A straight-forward method of estimating the series resistance from a solar cell is to find the slope of the IV curve at the open-circuit voltage point [32].

4.5 Shunt Resistance

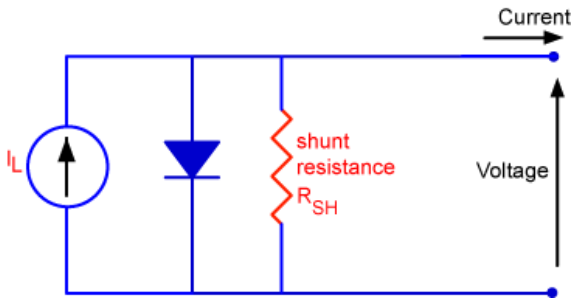

Fig. 4.5 Circuit diagram of a solar cell with shunt resistance

$$I = I_L - I_0 \exp[\frac{q(V + IR_s)}{nKT}] - \frac{V}{R_S H} \tag{4.7}$$

Where, I is the cell output current, I_L is the light generated current, V is the voltage across the cell terminals, T is the temperature, q and k are constants, n is the ideality factor, and R_sh is the cell shunt resistance. Significant power losses caused by the presence of a shunt resistance, R_{sh}, are typically due to manufacturing defects, rather than poor solar cell design. Low shunt resistance causes power losses in solar cells by providing an alternate current path for the light-generated current. Such a diversion reduces the amount of current flowing through the solar cell junction and reduces the voltage from the solar cell. The effect of a shunt resistance is particularly severe at low light levels, since there will be less light-generated current. The loss of this current to the shunt therefore has a larger impact. In addition, at lower voltages where the effective resistance of the solar cell is high, the impact of a resistance in parallel is large. An estimate for the value of the shunt resistance of a solar cell can be determined from the slope of the IV curve near the short-circuit current point. The effect of shunt resistance on I-V curve is shown in **Fig. 4.6** [33].

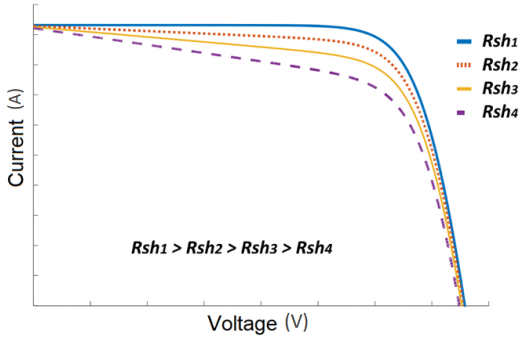

Fig. 4.6 Effect of shunt resistance on I-V curve

4.6 Shunt and series resistance calculation from dark I-V

By first charting the dark I-V characteristic, it is possible to determine the shunt and series resistance in a very practical manner. In this instance, it is possible to interpolate the characteristics around 0 voltage, where the I-V characteristics are a straight line. You can obtain the best fir straight line, where the inverse slope equals the shunt resistance. Then, we plot the I-V characteristics on a semi-log scale, which will result in a straight line in the middle current range, where the current is dominated by the exponential dependence. The semi-log I-V characteristic deviates from the straight line at high currents. The variation in voltage dV at a given current is caused by the voltage drop across the series resistance Rs. So,

$$R_s = \frac{dV}{dI} \tag{4.8}$$

4.7 Schottky barrier height

The Schottky barrier height is one of the most intriguing features of any metal-semiconductor (MS) contact (SBH). The SBH is the rectifying barrier for electrical conduction across the MS junction and, as such, is essential for the proper operation of any semiconductor device. The magnitude of the SBH represents the energy mismatch between the majority carrier band edge of the semiconductor and the Fermi level of the metal across the MS contact. At the interface of a metal and n-type semiconductor, the SBH is the difference between the minimum of the conduction band and the Fermi level. And for a p-type contact, the SBH is the difference between the maximum of the semiconductor's valence band and the Fermi level of the metal. FB is the most used symbol for the SBH.

Other superscripts and/or subscripts may be used to specify the type of semiconductor and whether or not the SBH refers to the flat-band or depletion condition. This is how

band diagrams are often created to depict the band bending for n-type and p-type semiconductors.

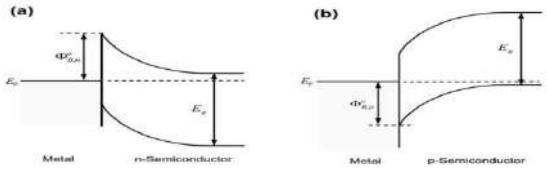

Fig. 4.7 Schottky barrier height

"Asymptotic band diagrams", which illustrate how the semiconductor (or metal) bands vary as the bands approach the MS interface. The region inside this little black box is

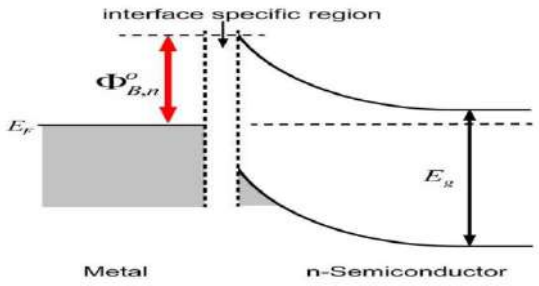

Fig. 4.8 Schottky barrier height

known as the interface specific region (ISR). This is the transitional region between the metal and the semiconductor, where magnitude of the SBH is determined.

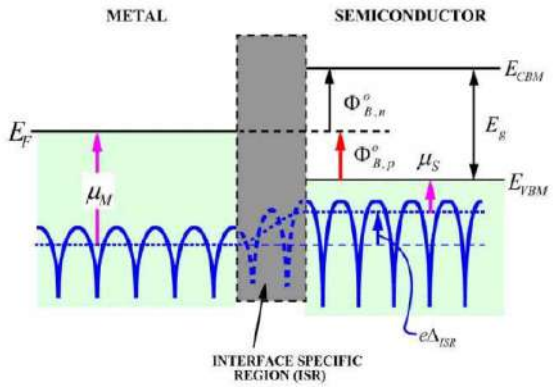

Fig. 4.9 Schottky barrier height

A term, "Fermi level (FL) pinning", has often been used to describe the insensitivity of the experimental SBH to the metal work function.

4.8 Ideality Factor

Ideality factor defines how good the diode is. It depends on, V, I, Temperature and junction quality. At room temperature higher value of ideality factor means the junction between two semiconductor or metal semiconductor junction is not good enough. The value of Ideality factor presents how closely the diode follows the ideal diode equation and can be determined from the slope of the linear region of the semi-log forward bias IâĂŞV characteristics by using equation given below:

$$n = \frac{q}{KT}(\frac{dV}{dlnI}) \tag{4.9}$$

here K is the Boltzmann's constant, q is the elementary charge, T is the absolute temperature in K, $\frac{dV}{dlnI}$ is slope of (I-V) curve.

1. Ideality factor is equals to unity for an ideal diode. However, n has usually a value greater than unity. High values of n can be attributed to the presence of the interfacial thin native oxide layer and a wide distribution of low-SBH patches (or barrier inhomogeneities), series resistance effect and therefore, to the bias voltage dependence of the SBH [34].
2. The analysis of the I-V characteristics based on application of the thermionic emission theory reveals an abnormal an increase in the ideality factor and decrease in the barrier height with a decrease in temperature [35].
3. The ideality factor n is a measure of conformity of the diode to pure thermionic emission. the higher values of n could be attributed to the presence of a wide distribution of low-SBH patches caused by lateral barrier inhomogeneities. Also, the image-force effect, recombination-generation, and tunneling may be possible mechanisms that could lead to the ideality factor value greater than unity [36].
4. The reason of larger value of ideality factor from unity is due to high series resistance and generation/recombination currents in depletion region
5. The higher values of n may be attributed to factors such as interfacial layer thickness, leakage, shunting, bulk series resistance, or any resistive loss [37]

There are several practical problems when measuring Ideality factor:

1. At low voltages the shunt resistance (R_{shunt})dominates the device performance and causes a large peak. It is usually not possible in practice to correct for the effects of R_{shunt}.
2. At high voltages in a dark-IV curve the series resistance dominates and this causes a large peak in the ideality factor curve at high voltages. This can be alleviated by using the Suns-V_{oc} curve that as noted earlier gives a curve the same as dark IV but without the effects of series resistance.
3. The ideality factor comes from the differential of a signal so it is very prone to noise. Noise problems are particularly problematical in Suns-V_{oc} measurements. To reduces noise the slope is usually taken as a fit over several points.
4. The effects of temperature are a problem particularly if the temperature change during the measurement.

CHAPTER 5
EXPERIMENTAL STUDY

5.1 Introduction

A semiconducting material which is extensively studying to utilize in the preparation of DSSC is Zinc Oxide and is the competitor of TiO_2 (because of its properties such as nearly equal to band gap as that of TiO_2, great transparency and easy to fabricate with different nanostructured films. Recently, with various nanostructures: nanowires, nanorods, nanoflowers, or nanosheets have garnered attention due to excellent optical, electrical and structural properties [1].

5.2 Experimental Procedure

5.2.1 Photoanodes preparation

For giving the suspension for electrophoretic deposition,20 wt.% ZnO nanoparticle and 4 vol% water are mixed with 100 ml ethanol. At 70% amplitude,a homogenizer named Sonic VCX-130 has been used to disperse ZnO NP inside the suspension for 10 min. Moreover, a material,tin oxide, coated with Fluorine doped (FTO) glass substrate which was used to make photoelectrode of the film. In this research, acetone is used to clean the electrodes twice. Likewise, Mithanol is used once for cleaning and then the substrates are dried by nitrogen flow followed by UV-03 cleaning.cathode is made from FTO substrate and anode is made from titanium sheet where the substrates are 2ÃŮ2 cm^2 with area.Electrode's applied biasing potential was 60V DC maintaining a 2.5 cm distance between them.In two ways,The deposition was performed within 4 min.After deposition ,the photoanode was dried at 80Âř C temperature with a hot plate for a few minutes.Lastly,when the second deposition was completed,the photoanodes were dried again

5.2.2 Post-treatment

Hot-compress, a postdepostion treatment, is used on the deposited films with suited temperature along with a pressure machine known as Mini Test Press-10.In this process, compression temperature at the range of room temperature to 110 oC and 130MPa compression pressure are the two factors that are used in the preparation of the flims.

5.2.3 Cell fabrication

The fabrication and the characterization part has been conducted in Soga-Kishi Lab, Nagoya Institute of technology. The whole experimental investigation has been conducted by Dr. M. S. H. Choudhury [38].

For preparing dye loading,An ethanol solution was produced with the mixture of 0.3 mM Ru complex dye N719.The preparing photoanodes were dipped into dye for the duration of 1 hour pt-coated glass counter electrode and iodide/triiodide redox were used to fabricate the cells in the following step.For creating a gap, a polymer film was used in the middle of the electrodes. So as to, it is possible to confine the electrolyte within the cells.In our experimentation, the area of the resulting active cell was 0.16 cm^2 and the thickness of the film was 12 to 17μm which was dependent on the variation of the compression temperature.For graphing the I-V characterization, a standard solar spectrum of an air mass of 1.5 with 100 mW cm-2 was used.By applying solar simulator and profilometer the properties of Photovoltaic and the thickness of the film were measured .

CHAPTER 6

RESULT AND DISCUSSION

6.1 Introduction

In this chapter, we shall discuss the result of this analysis and discuss all the resultant factors and operations of this system. We shall look after some graph, curves, and other characteristics results from this segments.

6.2 Result Analysis

6.2.1 Conventional Method

Dark (I-V) parameters under forward and reverse bias at room temperatures for the diode can be obtained by semilogarithmic plot is obtained by Converting current(I) into log(10). **Fig 6.1** shows the lnI(mA) vs Voltage curve based On dye Loading time.

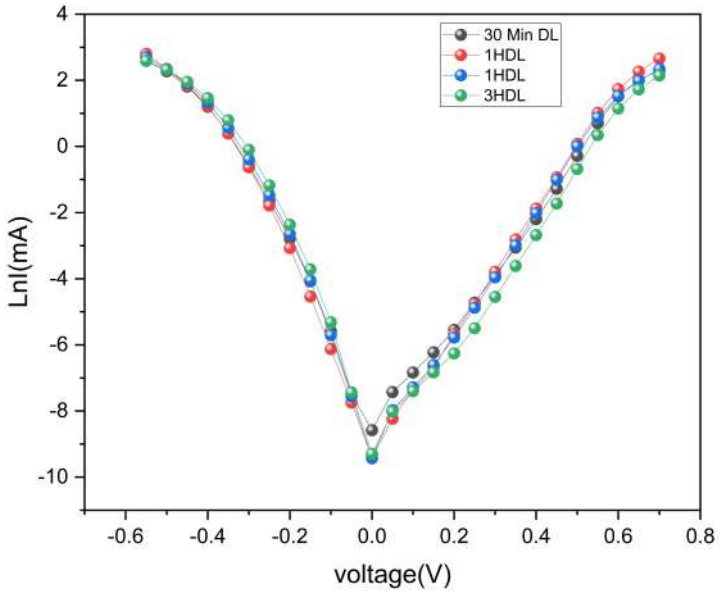

Fig. 6.1 Dark (lnI-V) Curve Based on Dye Loading time

Using Equation 3.6,3.7 and 3.8 , The Experimental values of T_s, φ_{b0} and n for room temperature are determined from the intercept and slope of lnI vs V Relation at low forward Applied voltage [39].

6.2.2 Ideality factor

We know that,

$$n = \frac{q}{KT}\frac{dV}{d\ln(I)} \tag{6.1}$$

Where,

q=$1.6 * 10^{-19} Jk^{-1}$,K=$1.38 * 10^{23} kg^{-2}k^{-1}$, T=298K, $\frac{dV}{dlnI} = 0.1499$

$$n = \frac{1.6 * 10^{19}}{1.38 * 10^{-23} * 298} * 0.1499 = 2.583 \tag{6.2}$$

The ideality factor for separate Dark(I-V) data is obtained by taking individual slope of (lnI-V) Curve, that are included Table.

6.2.3 Saturation Current

At low and intermediate voltage region, by using equation 3.6, the plot of (lnI-V) is linear and the extrapolationg of this plot to lnI axis gives the reverse saturation current is I_s.

6.2.4 Zero bias Barrier Height

we know that, Zero bias barrier height

$$\varphi_{b0} = \frac{K_b T}{q} \ln(\frac{AA_* T^2}{I_s}) \tag{6.3}$$

Where,

q=$1.6 * 10^{-19} Jk^{-1}$,K=$1.38 * 10^{23} kg^{-2}k^{-1}$, T=298K, A=0.16 Cm^2

A^*=3.2*10^9 A/Cm^2k^2, I_s=1.2491*10^-3A

$$\varphi_{b0} = \frac{1.38 * 10^{-23} * 298}{1.6 * 10^{-19}} \ln(\frac{0.16 * 3.2 * 10^9 * 298^2}{1.2491 * 10^{-3}}) = 1.0255ev \tag{6.4}$$

The saturation currents, ideality factor and the zero-bias barrier height values obtained by using conventional (I-V) method are showed in following table.

Table 6.1 The saturation currents, ideality factor and the zero-bias barrier height values obtained by using conventional (I-V) method

Dye Loading Time	Temperature	Saturation Current	Ideality Factor
30Min	298K	$2.1293*10^{-4}$	2.53
1HDL	298K	$1.0228*10^{-4}$	2.10
2HDL	298K	$1.0214*10^{-4}$	2.20
3HDL	298K	$1.0860*10^{-4}$	2.50

6.2.5 Series And Shunt Resistance from dark IV Curve

We utilized the traditional method to measure the effect of series resistance and shunt resistance on the solar cell in the dark. We may determine the junction resistance using I-V curves, where Rj=$\frac{dv}{di}$. Both series resistance and series resistance are represented by Rj. **Fig 6.2** shows the plot of junction resistance (Rj) against the applied voltage(V). we can determine shunt resistance from Rj versus Voltage(V) plot. Similarly, we can also determine series resistance from Rj versus Voltage(V) plot, for forward bias potential. Series resistance and shunt resistance determined from graph(5.2) R_s= 373.78(ohm), R_{sh}= =266666.10(ohm) [40].

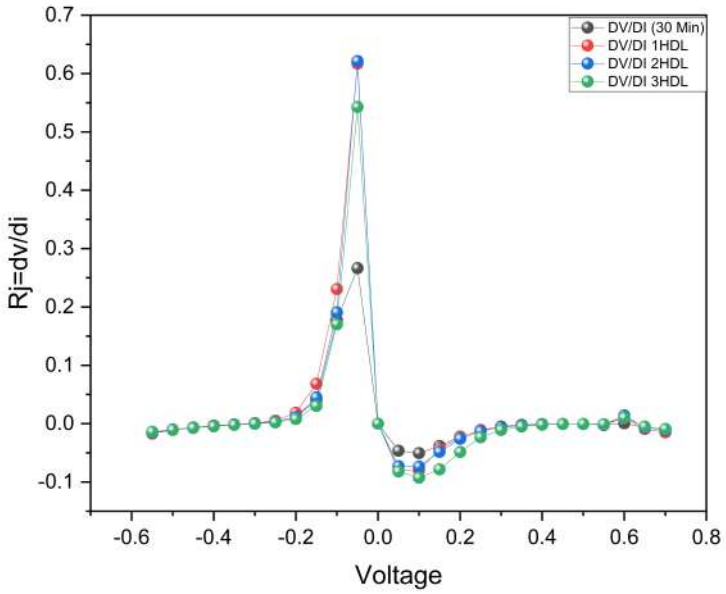

Fig. 6.2 Series and shunt Resistance values obtained by using conventional I-V

Table 6.2 Series and shunt Resistance values obtained by using conventional I-V method

Dye Loading Time	Rs(ohm)	Rsh(ohm)
30MIN	373.78	266666.10
1HDL	310.75	617054.98
2HDL	311.52	621426.27
3HDL	312.32	542651.79

According to **Table-6.2**, the 1hr Dye loading time cell has the lowest value of series resistance. The shunt resistance from the other cell is also relatively high. As a result, we can conclude that, according to Conventional methods, will outperform other cells.

6.2.6 Cheung Method

First we took Forward bias I-V data of dark condition. Then we plot LnI-V curve(**Fig 6.3**) Based on Dye loading time.

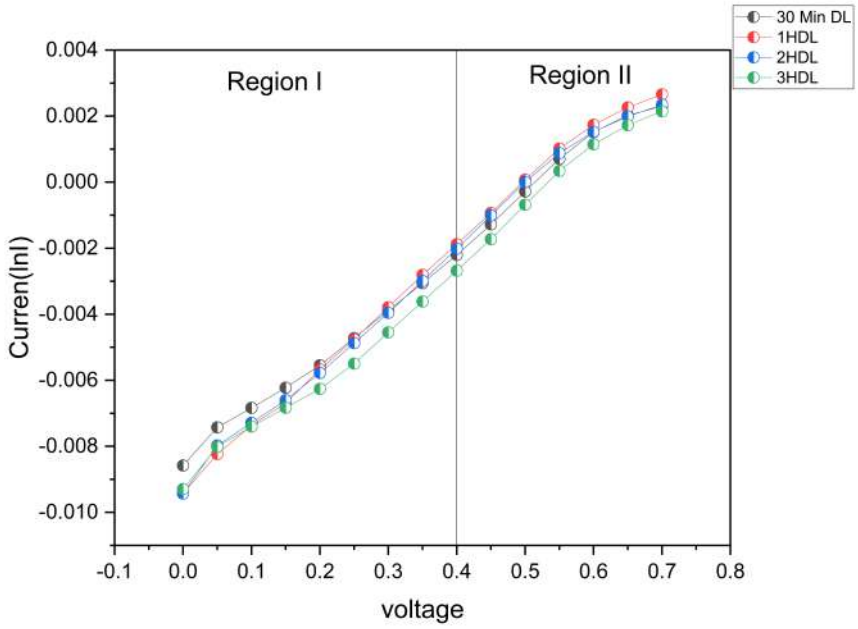

Fig. 6.3 Dark (lnI-V) Curve forward bias Based on Dye Loading time

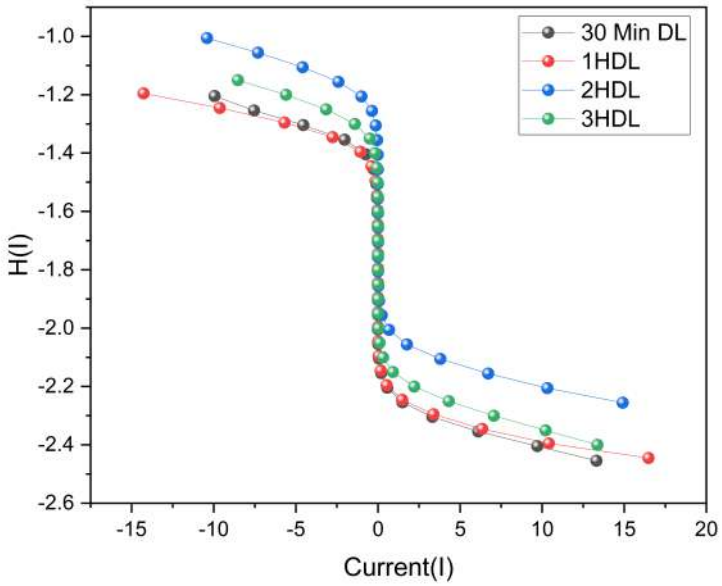

Fig. 6.4 H(I)vs current(I) plot

From equation 3.9,a plot of $\frac{dV}{dlnI}$ against I(A) should yield a straight line in the downward curvature region of the (I-V) characteristic with an intercept and slope giving the value of n and R_s respectively.

We know that,

$\frac{dV}{dlnI} = IRs + \frac{nKT}{q}$

$\frac{dV}{dlnI} = 61.76I + 0.0542135$

6.2.6.1 Series Resistance

Where Rs =61.76(ohm) Similarly, some value of series resistance was taken from the d(v)/d(lnI) against I(A) which are include in the **table 5.3** given below

6.2.6.2 Ideality Factor

Here,

$$\frac{nKT}{q} = 0.0542135 \tag{6.5}$$

$$n = \frac{0.0542135 * 1.6 * 10^{-19}}{1.38 * 10^{-23} * 298} = 2.11 \tag{6.6}$$

from equation 3.10,3.11 we determine H(I) and zero barrier height(Φ_b). them plot H(I) vs Current(I) plot. **Table 6.3** contain the of R_s,n and φ_b according to dye loading time.

Table 6.3 Ideality factor and Series Resistance values obtained by using CheungâĂŹs method

Dye Loading Time	Rs(ohm)	Ideality factor(n)	Zero Barrier Height
30MIN	61.76	2.11	1.64
1HDL	55.84	2.10	1.63
2HDL	57.57	1.89	1.44
3HDL	59.31	2.05	1.58

According to the Cheung function approach, the value of series resistance of the 1hr dye loading time cell is less than that of the other cells. As a result, we may conclude that the 1hr dye loading time cell will outperform the other cells.

6.3 Norde Plot

In **fig 6.5** depict F(V) vs voltage plot. here f(V) Calculated from equation 3.12. from the value F(V) we take the minimum value F(V_o) of F(V) and alse take their corresponding Voltage(V_o) and Current(I_o). finally apply this value in equation 3.13 and 3.15 to determne the value of R_s and φ_b.

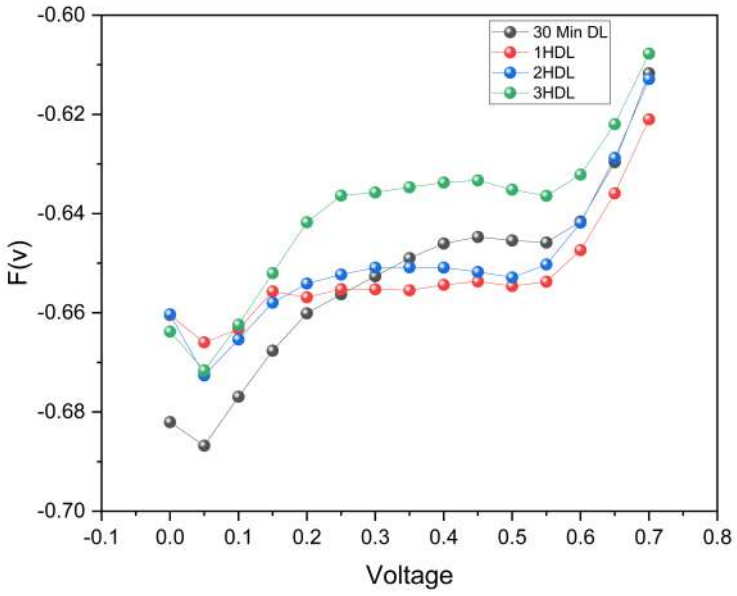

Fig. 6.5 F(V) vs Voltage(V) plot in forward bias potential

Table 6.4 Ideality factor and Series Resistance values obtained by using Norde plot method

Dye Loading Time	R_s	Zero Barrier Height(φ_b)
30min DL	1.93	1.544
1HDL	1.56	1.550
2HDL	1.72	1.547
3HDL	4.81	1.545

6.3.1 Generialized norde plot

It is the modified version of norde plot method. From equation 3.16,3.17 and 3.18 we can determine series resistance and zero barrier height. here we took the value of α double of n (which is determine in conventional method).

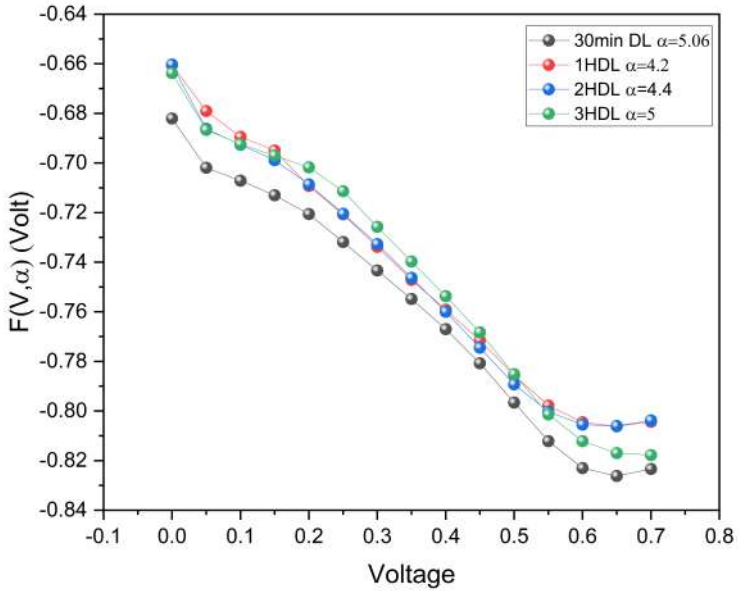

Fig. 6.6 F(V,α) vs Voltage(V) plot in forward bias potential

Table 6.5 Ideality factor and Series Resistance values obtained by using generilized Norde plot method

Dye Loading Time	R_s	Zero Barrier Height(φ_b)
30min DL	4.86	1.21
1HDL	3.28	1.11
2HDL	3.79	1.25
3HDL	4.81	1.08

According to a generilized norde plot, the series resistance value of a cell with a 1hr dye loading period is less than that of other cells. Therefore, this cell provides superior

performance to other cells.

6.4 I-V data Under Illumination

Using a solar simulator, we gather I-V data under illuminating conditions. The determination of the dc current-voltage characteristic under various intensities of white light illumination is one of the standard techniques for characterizing photovoltaic cells. In order to test the photo response of the prepared ZnO-based DSSCs, a sample was exposed to a high-power tungsten lamp from a safe distance to prevent thermal heating of the cell. This graph depicts the fourth quadrant region of the (I-V) measurements at various illumination intensities. The photocurrent and photovoltage clearly increased with increasing illumination. It is believed that the dye sensitization of semiconductor materials produces high photovoltages but low photocurrents. This is caused by particle agglomeration and self-quenching primarily. Using Lambert W Function we determine series resistance and shunt resistance of the cell based on different dye loading time.

6.4.1 Series And Shunt Resistance

The resistance of the solar cell is one of the primary factors that might affect the total power conversion efficiency of DSSC. There are two types of resistance that can have an impact on efficiency. The Series resistance and Shunt resistance can be calculated using the DSSC's I-V characteristic as shown in figure.

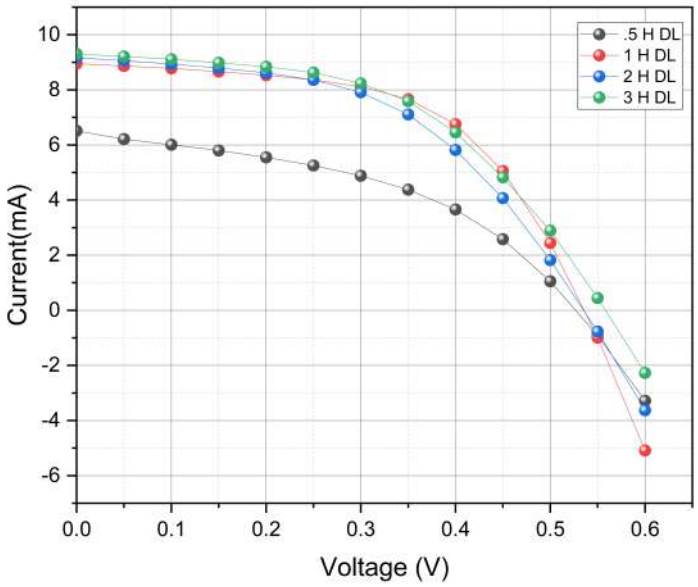

Fig. 6.7 Current versus Voltage plot under illumination

Table 6.6 Series and shunt Resistance values Under Illumination

Dye Loading Time	Rs(ohm)	Rsh(ohm)
30MIN	17.25	126.45
1HDL	8.12	143.82
2HDL	16.01	263.67
3HDL	14.54	173.45

In **table 6.6**, list the R_s and R_{sh} values of the cell under various lighting conditions and dye loadings. The series resistance of the 1hr dye loading time cell is lower than the series resistance of other cells, while the shunt resistance is about higher. Therefore, the 1 hour dye loading time cell performs better than other cells.

CHAPTER 7
CONCLUSION

7.1 Conclusion

To Analysis the effect of dye loading on DSSC,we analysis the I-V data of dark and illumination condition. in this investigation we use conventional method, cheung function method, norde plot method, generilized norde plot method, Lambart W Function and determinr series resistance, shunt resistance , ideality factor, saturation current, zero barrier height of the cell.

we analysis the performance of cell based on series resistance. The cell which have lowest series resistance, give better performance from other cell. the output parameter of cell vary from method to method but we find lowest value of a cell in all applying method.

The performance analysis based on different dye loading time using I-V data under dark and illumination condition are very impactful. Here use electrophoretic deposition technique for cell fabrication process.

After analyzing all of the data, we've determined that cells with a 1 hour dye-loading time cell give better performance with the conversion efficiency of 2.700500%, short circuit current density of 8.954375 (mA/cm^2) ,open circuit voltage(V_{oc}) of 0.535590 (V), Fill factor(FF) of 0.563087.

7.2 Future Work

The best conversion efficiency of 2.70% for room temperature with 1hour dye loading time is highlighted in this investigation. Though this efficiency result is not worthy of large scale production obtained for ZnO based DSSC still this efficiency may encourage the researchers.

1) To use a new dye sensitizer to increase the efficiency and stability of DSSC for better photoelectric conversion efficiency.

2) Develop counter electrode with better dye absorbance.

REFERENCES

[1] L. P. Joshi, Y. Poudel, M. L. Nakarmi, P. R. Niraula, and S. P. Shrestha, "Preparation and characterization of zinc oxide based photoanode for dye-sensitized solar cell using delonix regia natural dye extract," *Journal of Nepal Physical Society*, vol. 4, no. 1, pp. 1–6, 2017.

[2] J. Gong, K. Sumathy, Q. Qiao, and Z. Zhou, "Review on dye-sensitized solar cells (dsscs): Advanced techniques and research trends," *Renewable and Sustainable Energy Reviews*, vol. 68, pp. 234–246, 2017.

[3] P. Teesetsopon, S. Kumar, and J. Dutta, "Photoelectrode optimization of zinc oxide nanoparticle based dye-sensitized solar cell by thermal treatment," *Int. J. Electrochem. Sci*, vol. 7, no. 6, pp. 4988–4999, 2012.

[4] S. Singh, A. Singh, and N. Kaur, "Imine-linked receptors decorated zno-based dye-sensitized solar cells," *Bulletin of Materials Science*, vol. 39, no. 6, pp. 1371–1379, 2016.

[5] T. Pauporté, "Optimizing light harvesting and charge collection in dye-sensitized solar cells based on zno," *ECS Transactions*, vol. 58, no. 11, p. 29, 2013.

[6] A. Bahadori, G. Zahedi, and S. Zendehboudi, "An overview of australia's hydropower energy: Status and future prospects," *Renewable and sustainable energy reviews*, vol. 20, pp. 565–569, 2013.

[7] W. Shockley and H. J. Queisser, "Detailed balance limit of efficiency of p-n junction solar cells," *Journal of applied physics*, vol. 32, no. 3, pp. 510–519, 1961.

[8] M. Green, E. Dunlop, J. Hohl-Ebinger, M. Yoshita, N. Kopidakis, and X. Hao, "Solar cell efficiency tables (version 57)," *Progress in photovoltaics: research and applications*, vol. 29, no. 1, pp. 3–15, 2021.

[9] A. M. Bagher, M. M. A. Vahid, and M. Mohsen, "Types of solar cells and application," *American Journal of optics and Photonics*, vol. 3, no. 5, pp. 94–113, 2015.

[10] J. Chandrasekaran, D. Nithyaprakash, K. Ajjan, S. Maruthamuthu, D. Manoharan, and S. Kumar, "Hybrid solar cell based on blending of organic and inorganic materialsâĂŤan overview," *Renewable and Sustainable Energy Reviews*, vol. 15, no. 2, pp. 1228–1238, 2011.

[11] B. O'regan and M. Grätzel, "A low-cost, high-efficiency solar cell based on dye-sensitized colloidal tio2 films," *nature*, vol. 353, no. 6346, pp. 737–740, 1991.

[12] A. Hagfeldt, G. Boschloo, L. Sun, L. Kloo, and H. Pettersson, "Dye-sensitized solar cells," *Chemical reviews*, vol. 110, no. 11, pp. 6595–6663, 2010.

[13] Y. Chiba, A. Islam, Y. Watanabe, R. Komiya, N. Koide, and L. Han, "Dye-sensitized solar cells with conversion efficiency of 11.1%," *Japanese journal of applied physics*, vol. 45, no. 7L, p. L638, 2006.

[14] A. Fujishima and K. Honda, "Electrochemical photolysis of water at a semiconductor electrode," *nature*, vol. 238, no. 5358, pp. 37–38, 1972.

[15] H. J. Snaith, "Estimating the maximum attainable efficiency in dye-sensitized solar cells," *Advanced Functional Materials*, vol. 20, no. 1, pp. 13–19, 2010.

[16] D. C. Look, "Recent advances in zno materials and devices," *Materials science and engineering: B*, vol. 80, no. 1-3, pp. 383–387, 2001.

[17] R. Kumar, A. Umar, G. Kumar, H. S. Nalwa, A. Kumar, and M. Akhtar, "Zinc oxide nanostructure-based dye-sensitized solar cells," *Journal of Materials Science*, vol. 52, no. 9, pp. 4743–4795, 2017.

[18] D. I. Florescu, L. Mourokh, F. H. Pollak, D. C. Look, G. Cantwell, and X. Li, "High spatial resolution thermal conductivity of bulk zno (0001)," *Journal of applied physics*, vol. 91, no. 2, pp. 890–892, 2002.

[19] A. Desai and M. A. Haque, "Mechanical properties of zno nanowires," *Sensors and Actuators A: Physical*, vol. 134, no. 1, pp. 169–176, 2007.

[20] L.-W. Lai and C.-T. Lee, "Investigation of optical and electrical properties of zno thin films," *Materials Chemistry and Physics*, vol. 110, no. 2-3, pp. 393–396, 2008.

[21] A. Umar and Y.-B. Hahn, *Metal oxide nanostructures and their applications*. American Scientific Publ. Los Angeles, CA, USA, 2010, vol. 3.

[22] J. Haynes, "Experimental proof of the existence of a new electronic complex in silicon," *Physical Review Letters*, vol. 4, no. 7, p. 361, 1960.

[23] M. Grätzel, "Photovoltaic and photoelectrochemical conversion of solar energy," *Philosophical Transactions of the Royal Society A: Mathematical, Physical and Engineering Sciences*, vol. 365, no. 1853, pp. 993–1005, 2007.

[24] M. Rani and S. Tripathi, "A comparative study of nanostructured tio2, zno and bilayer tio2/zno dye-sensitized solar cells," *Journal of Electronic Materials*, vol. 44, no. 4, pp. 1151–1159, 2015.

[25] H. S. Hafez, I. Yahia, G. Sakr, M. Abdel-Mottaleb, and F. Yakuphanoglu, "Extraction of the dssc parameters based tio2 under dark and illumination conditions," *Adv. Mater. Corros*, vol. 1, pp. 8–13, 2012.

[26] P. B. Pillai, A. Corpus Mendoza, M. De Souza, G. Bree, and D. Jeng, "Extraction of schottky barrier at the f-doped sno2/tio2 interface in dye sensitized solar cells," *Journal of Renewable and Sustainable Energy*, vol. 6, no. 1, p. 013142, 2014.

[27] H. Norde, "A modified forward i-v plot for schottky diodes with high series resistance," *Journal of applied physics*, vol. 50, no. 7, pp. 5052–5053, 1979.

[28] D. A. Aldemir, A. Kökce, and A. F. Özdemir, "The comparison of the methods used for determining of schottky diode parameters in a wide temperature range," *Sakarya Üniversitesi Fen Bilimleri Enstitüsü Dergisi*, vol. 21, no. 6, pp. 1286–1292, 2017.

[29] S. Sarker, H. W. Seo, and D. M. Kim, "Calculating current density–voltage curves of dye-sensitized solar cells: a straight-forward approach," *Journal of Power Sources*, vol. 248, pp. 739–744, 2014.

[30] E. Meyer, "Extraction of saturation current and ideality factor from measuring voc and isc of photovoltaic modules," *International Journal of Photoenergy*, vol. 2017, 2017.

[31] K. Zhu, S.-R. Jang, and A. J. Frank, "Impact of high charge-collection efficiencies and dark energy-loss processes on transport, recombination, and photovoltaic properties of dye-sensitized solar cells," *The Journal of Physical Chemistry Letters*, vol. 2, no. 9, pp. 1070–1076, 2011.

[32] A. Mashreghi and F. Bahrami Moghadam, "Effect of photoanode active area on photovoltaic parameters of dye sensitized solar cells through its effect on series resistance investigated by electrochemical impedance spectroscopy," *Journal of Solid State Electrochemistry*, vol. 20, no. 5, pp. 1361–1368, 2016.

[33] O. Amiri and M. Salavati-Niasari, "High efficiency dye-sensitized solar cells (9.3%) by using a new compact layer: Decrease series resistance and increase shunt resistance," *Materials Letters*, vol. 160, pp. 24–27, 2015.

[34] Z. Çaldıran, A. Deniz, Ş. Aydoğan, A. Yesildag, and D. Ekinci, "The barrier height enhancement of the au/n-si/al schottky barrier diode by electrochemically formed an organic anthracene layer on n-si," *Superlattices and Microstructures*, vol. 56, pp. 45–54, 2013.

[35] E. El-Menyawy and A. Ashery, "Current–voltage characteristics and inhomogeneous barrier height analysis of au/poly (o-toluidine)/p-si/al heterojunction diode," *Journal of Materials Science: Materials in Electronics*, vol. 25, no. 9, pp. 3939–3946, 2014.

[36] Ö. Güllü, S. Asubay, Ş. Aydoğan, and A. Türüt, "Electrical characterization of the al/new fuchsin/n-si organic-modified device," *Physica E: Low-dimensional Systems and Nanostructures*, vol. 42, no. 5, pp. 1411–1416, 2010.

[37] C. Tozlu and A. Mutlu, "Poly (melamine-co-formaldehyde) methylated effect on the interface states of metal/polymer/p-si schottky barrier diode," *Synthetic Metals*, vol. 211, pp. 99–106, 2016.

[38] M. S. H. Choudhury, N. Kishi, and T. Soga, "Hot-compression: An effective postdeposition treatment for electrophoretically deposited dye-sensitized solar cell," in *2016 Ieee 43rd Photovoltaic Specialists Conference (Pvsc)*. IEEE, 2016, pp. 1632–1637.

[39] A. Abuelwafa, A. El-Denglawey, M. Dongol, M. El-Nahass, M. Ebied, and T. Soga, "On the electrical characterization of platinum octaethylporphyrin (ptoep)/si hybrid device," *Applied Physics A*, vol.

124, no. 1, pp. 1–12, 2018.

[40] M. Shah, M. Sayyad, K. S. Karimov, and M. Maroof-Tahir, "Investigation of the electrical properties of a surface-type al/nipc/ag schottky diode using i–v and c–v characteristics," *Physica B: Condensed Matter*, vol. 405, no. 4, pp. 1188–1192, 2010.